HET HOBBY ★ EBERLY TELESCOPE

HET Technical Report #43

SST Setting and Tracking Analysis

F. B. Ray

Hobby * Eberly Telescope Project
McDonald Observatory
University of Texas
RLM 15.308
Austin, Texas 78712

April 5, 1994

A Joint Project of
The University of Texas at Austin, The Pennsylvania State University,
Stanford University, Ludwig-Maximilians-Universität München, and Georg-August-Universität Göttingen

SST setting and tracking analysis

F. B. Ray
The University of Texas McDonald Observatory
Austin, Texas 78712

Latest revision: June 24, 1994

1. Introduction

The following equations are derived in order to better understand the setting and tracking procedure for the SST as well as the steps necessary to define operational software for its use. The SST's tracking mechanism is based on a multi-axis gantry robot which will allow the line of sight, running through the primary mirror's center of curvature (COC), to be driven to follow image trajectories lying within a 12° square centered on telescope's central axis and rotated to any parallactic angle from 0° to 360°. Two orthogonal axes, labeled X and Y, form a planar 2D stage designed to follow the projection of a celestial object's image trajectory. Since the trajectory will in general be tilted with respect to the XY plane, a Z-motion is also necessary to synchronize a point in the robot (the rotation point RP) with a given trajectory point moving with a known ephemeral rate.

Because the payload of the gantry robot includes optics whose axis must be aligned with the line of sight, a ray defined by the primary mirror's center of curvature and the celestial object, 2-axis tilt is mandatory. In addition, instruments requiring alignment of an aperture with a particular image feature demand a rotation of the instrument chassis about the line of sight in synchronization with the image rotation.

It is important to distinguish between **parallactic angle** and **field rotation**. Parallactic angle is a static relationship between the gantry robot's XY coordinate system and the local projection of right ascension and declination, about the telecentric axis; field rotation occurs about the line of sight as the gantry robot follows a trajectory. For a given azimuth setting, parallactic angle will be fixed, and could even be locked by a braking mechanism if other provisions are made for field (and possibly light baffle) rotation.

A fixed square XY mechanism spanning the locus of a rotatable 12° square must be $12\sqrt{2} = 17°$ on a side, which as will be shown provides additional tracking space (and time) with predictable reductions in signal/noise and incident flux due to extremal vignetting. However, it may be an option worth exercising at azimuths near 180° where tracking time is more precious.

2. Setting

The following variable definitions apply to the tracking geometry, and are the same as used in TR940104[1], except that we will more often use the term "**T**elecentric **D**istance to the **E**quator", abbreviated *TDE*, interchangeably with δ_c:

rotation point (**RP**) - the point tracked by the Cartesian (XYZ) mechanism
t – sidereal time
p_c – parallactic angle of the tracking mechanism
$r(t)$ – distance from **RP** to the transit plane
$d(t)$ – distance to the projection of **RP** in the transit plane from the telecentric axis
$x(t)$ – distance of **RP** from the Y-axis of an XYZ mechanism whose XY plane is perpendicular to the telecentric axis

[1] F. B. Ray, "Tracker mechanism kinematics, servo, and top-level software design for a semi-transit telescope with fixed spherical primary mirror", SST technical report TR -940104.

$y(t)$ – distance of **RP** from the X-axis of an XYZ mechanism whose XY plane is perpendicular to the telecentric axis
F_S – radius of the tracking sphere
$\delta(t)$ – declination of the object (not, in general, constant)
$h_c(t)$ – hour angle with respect to the transit plane (may be non-linear)
δ_T – angular distance from the transit point to the equator, or declination at time of transit
δ_c – angular distance from the telecentric axis to the equator (also known as *TDE*)
H – angular distance from the telecentric axis to the meridian (telecentric hour angle)

Local site constants include the elevation (or altitude) a of the telescope's axis above the horizon and the site latitude Φ. Two simplifications based on the SST's fixed elevation are immediately possible:

$$P = \cos a \cos \Phi, \text{ and } Q = \sin a \sin \Phi. \quad (1)$$

Except for specific small mechanical setting errors, P and Q are nominally constant for a given SST design.

From a previous development[2], we may express *TDE* and H in terms of azimuth A, measured from due north (0°) and using clockwise as the positive sense:

$$TDE = \sin^{-1}(P \cos A + Q) \quad (2)$$

$$H = \sin^{-1}\left[\frac{\cos a \sin A}{-\cos TDE}\right] \quad (3)$$

plotted as follows:

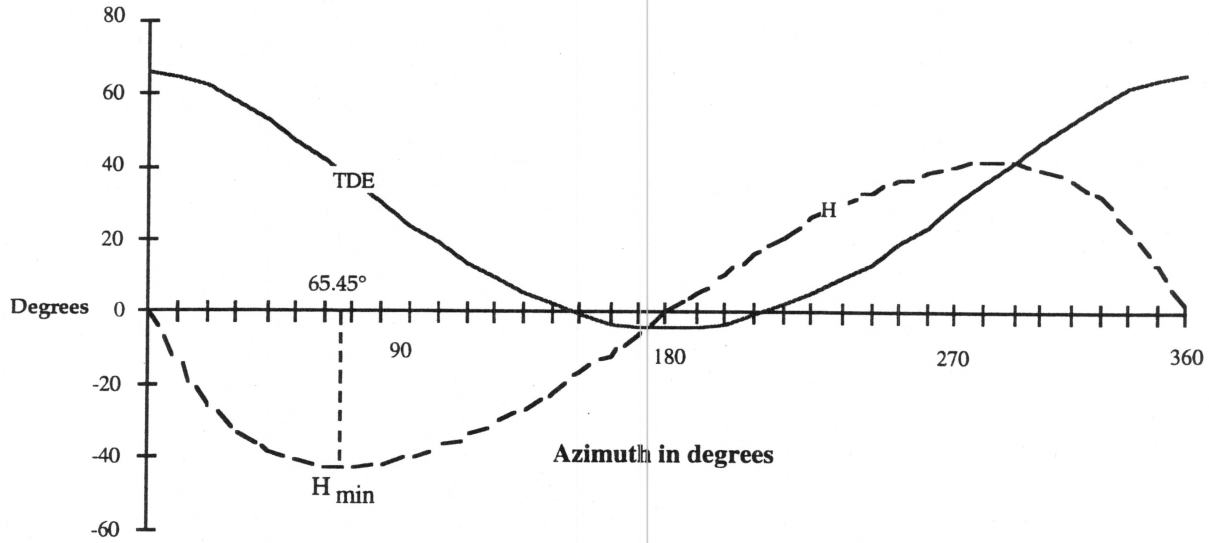

Figure 1. TDE and H as functions of azimuth angle A.

The value for H_{min} occurs[3] when $\cos A = \left[\frac{1-P^2-Q^2}{2PQ} - \frac{1}{2}\sqrt{\frac{1-P^2-Q^2}{PQ} - 4}\right]$. (4)

While equations 2 and 3 give the available ranges for H and *TDE*, setting the SST in azimuth will more often require deriving azimuth from a given TDE, inverting equation 2 to obtain

---

[2] ibid.

[3] F. B. Ray, "SST pointing error tolerances", SST technical report TR-083, February 1992.

$$A = \cos^{-1}\left[\frac{\sin TDE - Q}{P}\right] \tag{5}$$

whereupon

$$H = \sin^{-1}\left[\frac{\cos a \sin A}{-\cos TDE}\right] \tag{6}$$

and the principal value for the telecentric parallactic angle p_c is

$$p_c = \cos^{-1}[\cos H \cos A + \sin H \sin A \sin \Phi]. \tag{7}$$

The corresponding plot of A, H, and p, for both east and west azimuths, shows the close relationship between parallactic angle and azimuth. On the west side, we simply subtract the principal value of p_c from a full rotation.

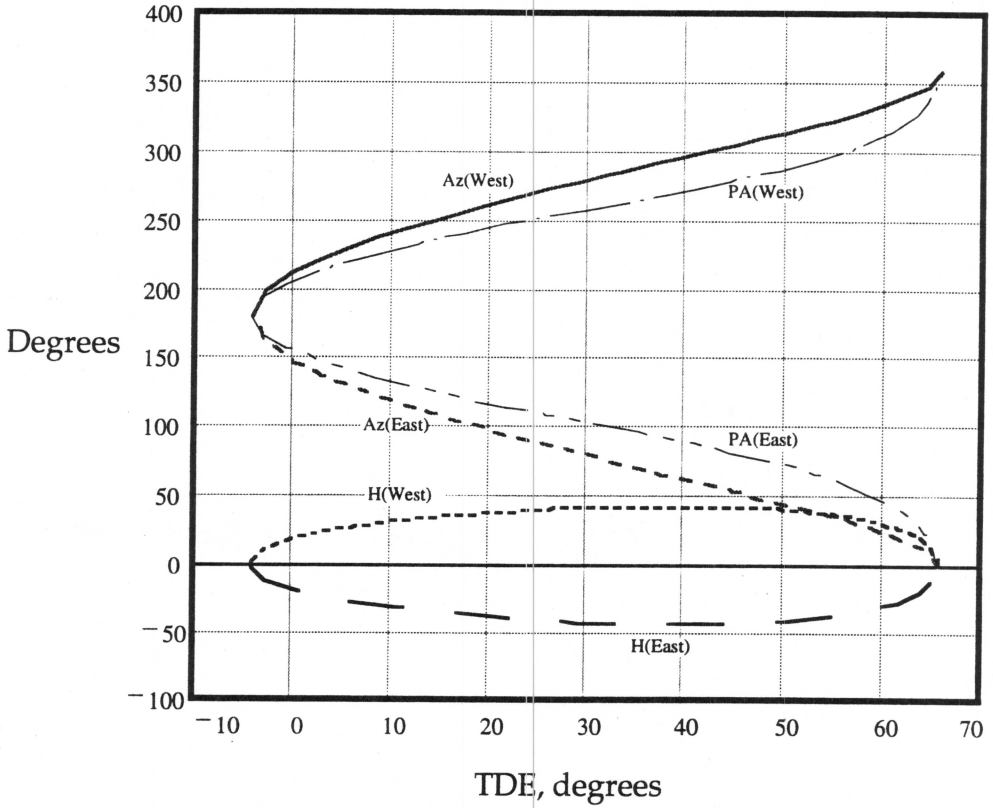

Figure 2. Telecentric hour angle H, azimuth A , and parallactic angle p_c as functions of TDE.

If a rotating stage were to strictly follow this definition of parallactic angle, it would need a range of not less than 360°. To utilize a rotating stage of some lesser range, closer to 180°, in order to minimize the length of the service loop to an instrument carried thereon, at least two other arrangements for the parallactic angle are possible.

The first alternative, illustrated in Figure 3, places the center of the parallactic angle travel at TDE = 38.5°, such that the ends of it are near A = 0° and A = 180°. In the following figure, when crossing to the west side from the east at either of these two positions, a 180° rotation of the parallactic angle is necessary to achieve its range on that side. The same is true when crossing from west to east. The disadvantage in this arrangement is that in the south, near azimuth 180°, the observer will need to subtract precious minutes, retracting the parallactic stage, from the available tracking time.

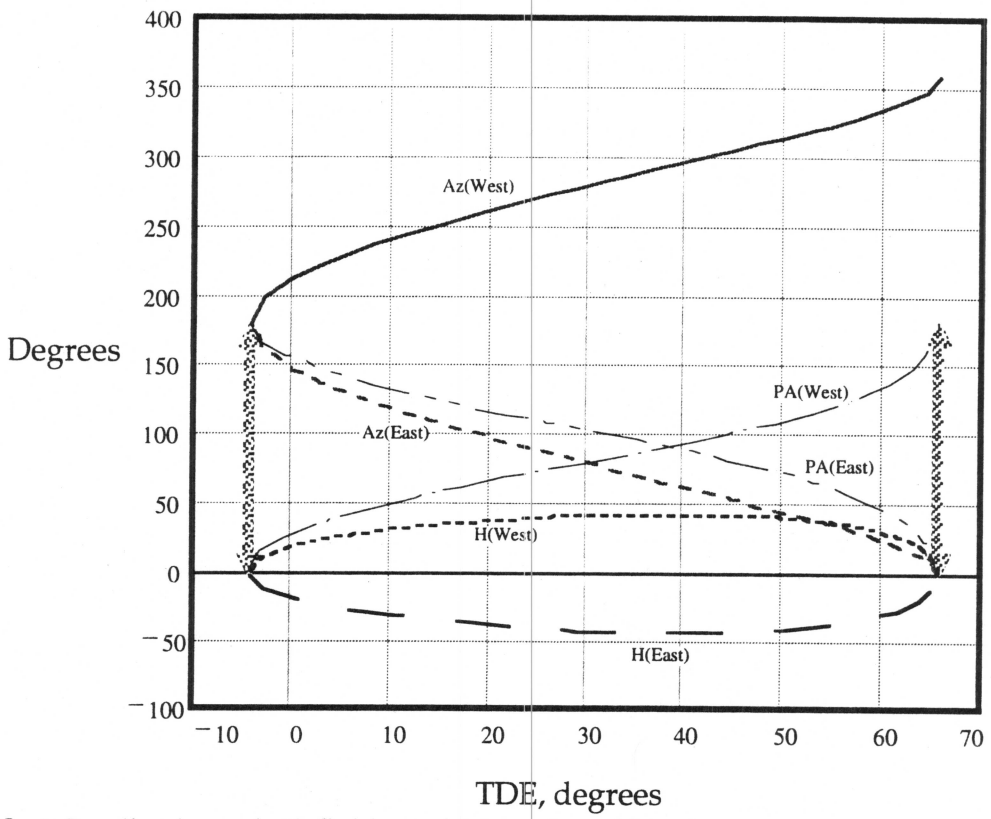

Figure 3. A Parallactic angle definition which prefers either the east or west side, but which requires a 180° retraction when making substantial crossings near A=0° and A=180°.

A second alternative, shown in Figure 4, adds a 90° phase angle to the parallactic angle definition, placing the center of its travel near A = 180°, (and A = 0°). A distinct advantage for southern declinations is that crossing A = 180° does not involve a 180° retraction for p. This is required, however, when $A \approx 60°$ and $A \approx 290°$.

In addition to the range needed to compensate for azimuth setting, instrument designers should anticipate alignment of instrument slits on the sky relative to various object feature orientations.

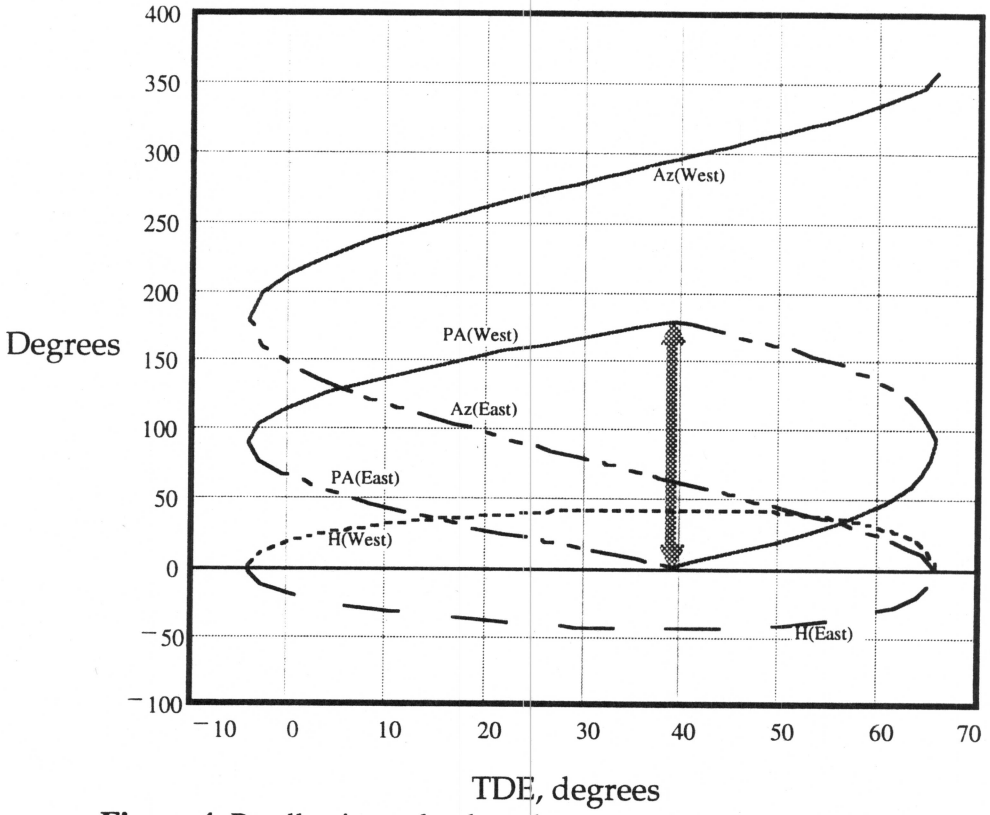

Figure 4. Parallactic angle phased to center it over $A = 180°$.

By substituting for H and A in equation 7, the principal value for p_c may be expressed as a function of TDE as follows:

$$p_c = \cos\text{-}1\left[\sqrt{1 - \cos^2 a \frac{\left[1 - \frac{(\sin TDE - Q)^2}{P^2}\right]}{\cos^2 TDE}} \frac{(\sin TDE - Q)}{P} - \cos a \frac{\left[1 - \frac{(\sin TDE - Q)^2}{P^2}\right]}{\cos TDE} \sin \Phi\right] \quad (8)$$

3. Tracking

3.1 Cartesian equations

In the SST report TR-940104, we have previously developed the following tracking equations:

$$x(t) = r(t) \cos p_c - d(t) \sin p_c \quad (9)$$

$$y(t) = r(t) \sin p_c + d(t) \cos p_c \quad (10)$$

where

$$r(t) = -F_S \cos \delta(t) \sin h_c(t) \quad (11)$$

$$d(t) = F_S [\sin(\delta_T - TDE) + \sin TDE \ (\cos \delta_T - \cos \delta(t) \cos h_c(t))] \quad (12)$$

the latter written with some "SST" constants for simplicity, as

$$d(t) = F_S [C5 - C2 \cos \delta(t) \cos h_c(t)] \quad (13)$$

using the following definitions for C5 and C2 (tracking constants fixed with azimuth):

$$C1 = \sin(\delta_T - TDE),\ C2 = \sin TDE,\ C3 = \cos\delta_T,\ C4 = C2\,C3,\ \text{and}\ C5 = C1 + C4. \quad (14)$$

From an angle β, the angular offset of the line of sight from the telecentric axis, given by

$$\beta(t) = \cos^{-1}[\sin TDE \sin\delta(t) + \cos TDE \cos\delta(t) \cos h_c(t)] \quad (15)$$

which, after defining a tracking constant $C6 = \cos TDE$, we may rewrite as

$$\beta(t) = \cos^{-1}[C2 \sin\delta(t) + C6 \cos\delta(t) \cos h_c(t)] \quad (16)$$

we may calculate the z displacement as a function of time

$$z(t) = F_S\,[1 - \cos\beta(t)] \quad (17)$$

or, alternatively

$$z(t) = F_S - \sqrt{F_S^2 - x^2 - y^2} \quad (18)$$

and two projected angles of tilt

$$\theta(t) = \tan^{-1}\left[\frac{y(t)}{F_S \cos\beta(t)}\right] \quad (19)$$

$$\phi(t) = \tan^{-1}\left[\frac{x(t)}{F_S \cos\beta(t)}\right]. \quad (20)$$

Rotation of the field about the line of sight while tracking is given by

$$\rho(t) = -\sin^{-1}[\sin\delta(t) \sin h_c(t)] \quad (21)$$

which does not depend on *TDE*.

Figure 5 illustrates the spherical geometry for the relations above.

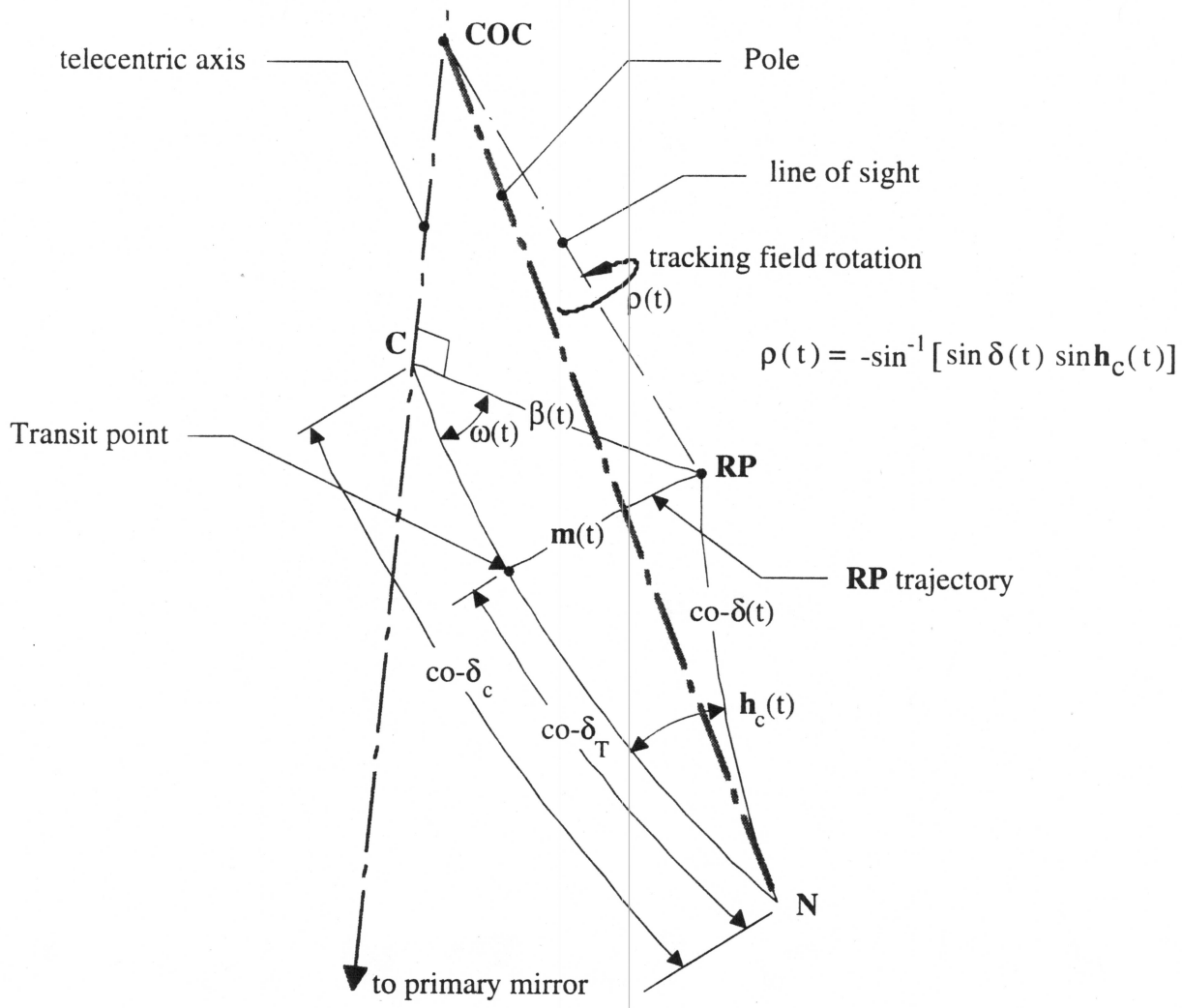

Figure 5. Spherical triangles used to develop the SST's tracking variables. The notation co-x is an abbreviation for the complementary angle of x, or 90° - x. The **RP** trajectory does not, in general, lie along a great circle, although that is the case when $\delta_T = 0$ and declination is constant. Point **C** is the intersection of the telecentric axis with the tracking sphere. **N** is the north pole on the tracking sphere, and **RP** is the (tracked) rotation point. For SST tracking, transit hour angle $h_c(t)$ is measured from the transit plane, which contains **N** and **C**. The **RP** trajectory and field rotation are symmetric with the transit plane.

3.2 Spherical geometry

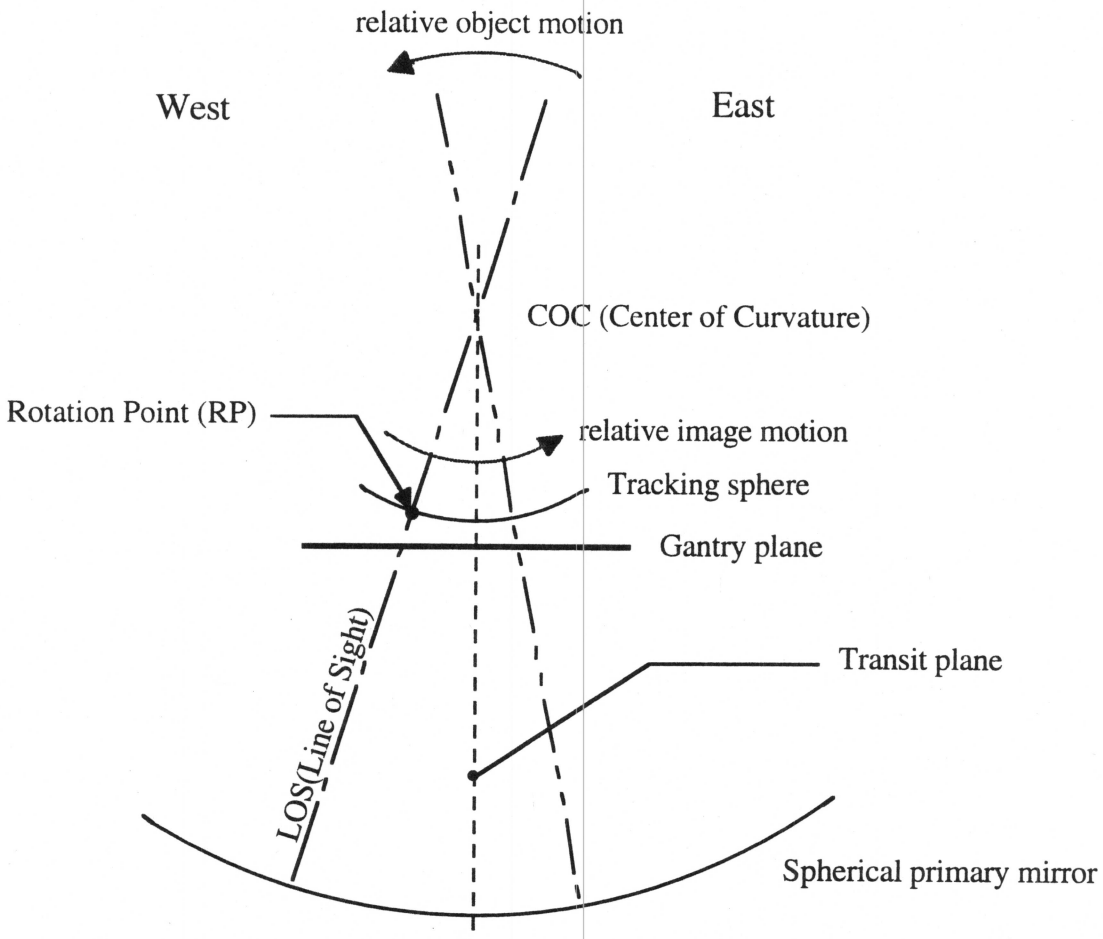

Figure 6. The spherical tracking principle for a fixed primary.

Since a spherical primary mirror has no preferred axis, one mode of tracking is to keep the mirror stationary with respect to the earth and drive a receiving head, which follows the line of sight to an object, along a spherical focal surface until the vignetting becomes unacceptable. Figure 6 illustrates the possibility of compensating for the Earth's rotation by tracking a "rotation point" RP along a trajectory generated by the object's relative motion. Such a scheme has certain advantages for constructing the primary mirror. The "gantry plane" indicates a mechanical plane where a large XY stage will be placed. By driving a mechanism in this plane, offsetting in Z, perpendicular to X and Y, and finally tilting a device about the rotation point (in 2 axes), the line of sight may be kept normal to the primary mirror. A surface we will call the "tracking sphere" will always contain the rotation point RP.

For real-time aperture alignment along an object feature such as a galactic axis, it is also necessary to provide a mechanism for rotation about the line of sight.

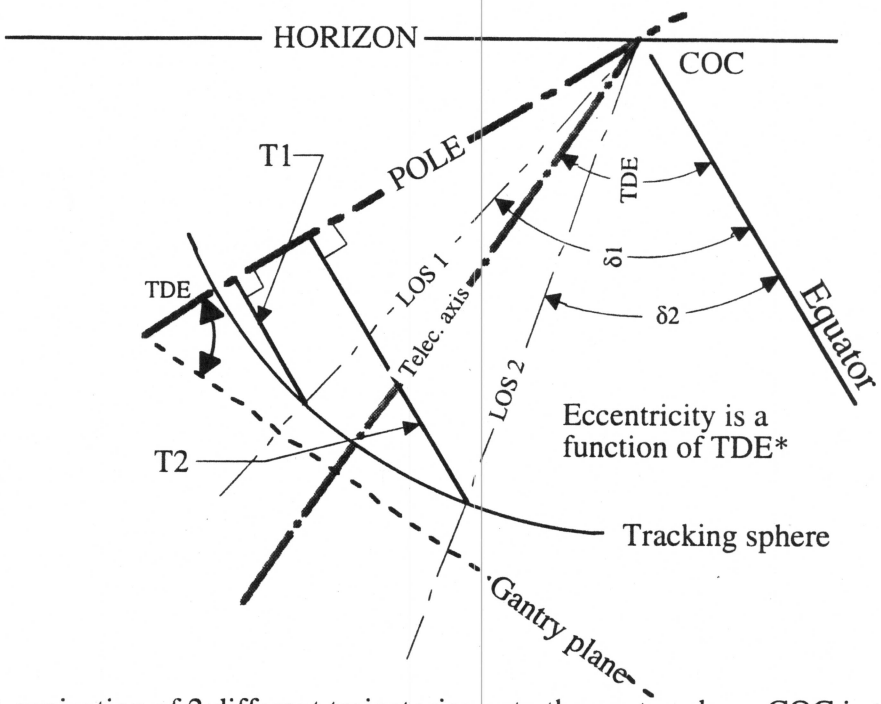

Figure 7. A projection of 2 different trajectories onto the gantry plane. COC is the center of curvature of the primary mirror.

An orthogonal view, showing the horizon and the pole in true length (Figure 7) illustrates the projection of trajectories T1 and T2 for the same *TDE*. Note that for sidereal objects, the trajectories are circular; therefore their projections onto the gantry plane are elliptical, with elliptical eccentricity equal to cos*TDE*.

Four azimuth positions, A = 0°, A = 40°, A = 120°, and A = 180°, are shown in Figure 8. Near the 120° position a small plane indicates the transit plane for that particular azimuth. In Figure 9 a view from zenith clearly shows the types of trajectories generated.

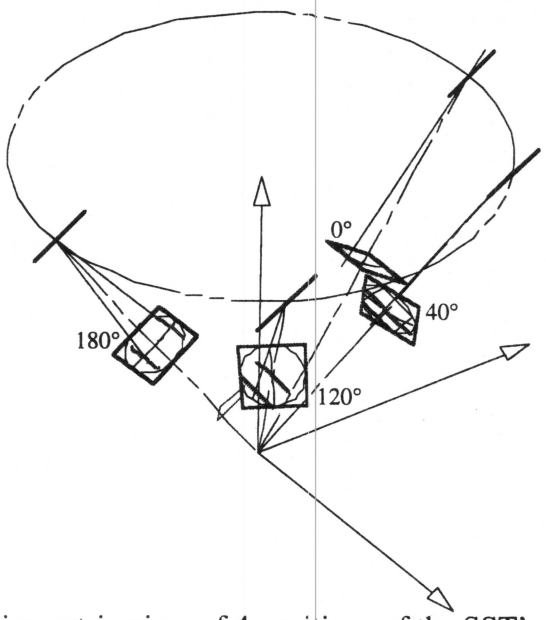

Figure 8. An isometric view of 4 positions of the SST's gantry plane.

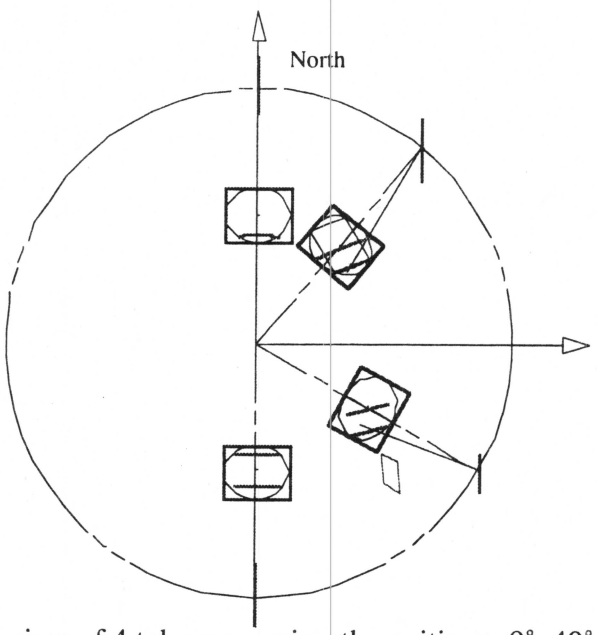

Figure 9. Zenith view of 4 telescope azimuth positions: 0°, 40°, 120°, and 180°.

Figure 10 illustrates examples of the various trajectories viewed from the center of curvature.

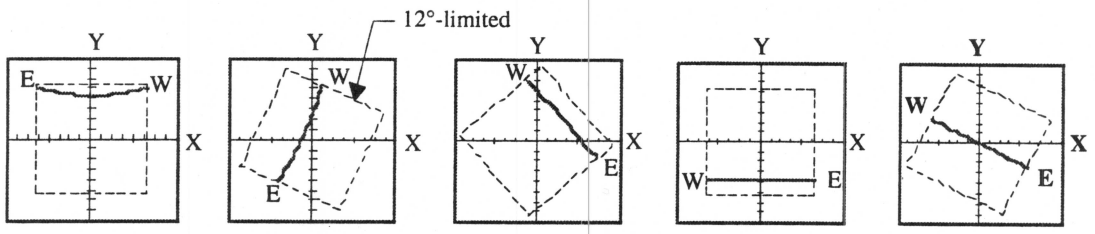

Figure 10. Various SST trajectories viewed from the COC. Since the zenith angle is not equal to the latitude, at azimuth 180°, the equatorial trajectory ($\delta = 0°$) does not cross the telecentric axis. However, we can force that condition by choosing $A \approx 147.9°$. The parallactic angle is the rotation of the dotted field relative to the solid border, and has the standard "sense".

The anatomy of an SST trajectory is illustrated in Figure 11. Note that for no extra mechanical tilt, the trajectory may be extended to a 17° ($\approx 12\sqrt{2}°$) circle, since there are trajectories which extend across the diagonal of the 12° square. The time of transit is defined as that time when RP crosses the transit plane (at the transit point). As we shall see, however, there is an appreciable additional vignetting penalty for this excursion.

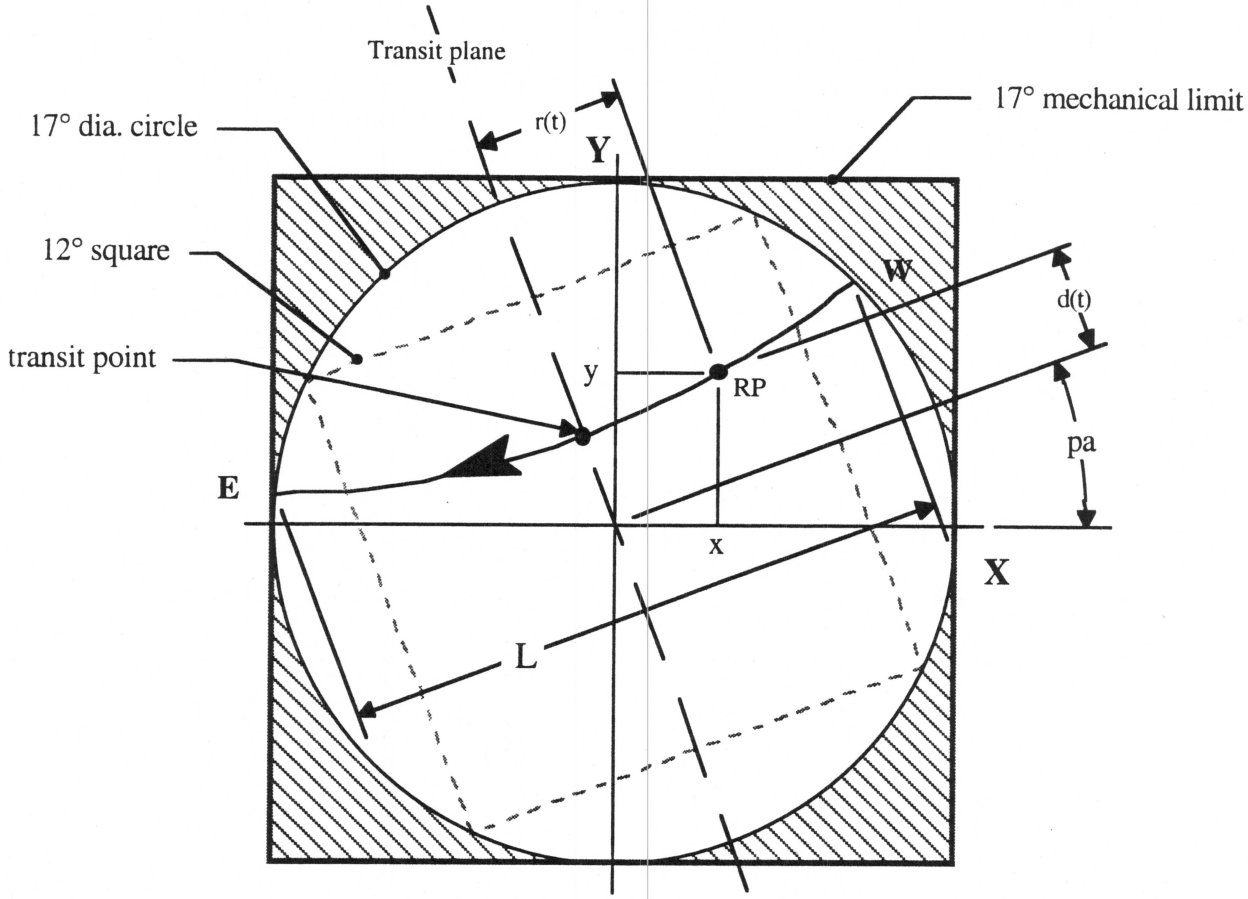

Figure 11. The (r, d) and (x,y) coordinate pairs are shown relative to the transit plane and the gantry XY coordinate system, respectively. For this trajectory, declination = 67°, azimuth = 10°, parallactic angle = 20.416°, and TDE = 64.65°. The image moves from west to east.

3.3 Available tracking time

The dimension L may be used to compute the available tracking time ATT, given a particular telescope setting and object declination. If we project a sidereal trajectory as an ellipse, it has the symmetrical form

$$\frac{r^2}{a^2} + \frac{d^2}{b^2} = 1 \tag{22}$$

where, for a tracking sphere of radius F_S,

$$a = F_S \cos(\delta_T) \quad \text{and} \quad b = F_S \cos(\delta_T) \sin(TDE) \tag{23}$$

and since the center of the ellipse is at the pole, we may express d in terms of r as

$$d = b\left[1 - \frac{\sqrt{a^2 - r^2}}{a}\right] + c \tag{24}$$

if, recalling the definition of the tracking constants C5 and C2,

$$c = F_S \left[C5 - C2 \cos(\delta_T) \right]. \tag{25}$$

The radius of the limiting circle is given by

$$r_{max} = F_S \sin(6\sqrt{2}^\circ) \tag{26}$$

therefore a point of intersection between the trajectory's elliptical projection and the limiting circle must also satisfy the circular form

$$r^2 + d^2 = r_{max}^2. \tag{27}$$

Solving for r and substituting in equation 24 we find

$$d = b\left(1 - \frac{\sqrt{d^2 - r_{max}^2 + a^2}}{a} \right) + c \tag{28}$$

and also that after rearranging, squaring, and collecting terms, d must be a root of the quadratic polynomial

$$(a^2 + b^2) z^2 + \left[-2a^2 (b + c) \right] z + a^2 c^2 + 2a^2 b c + b^2 r_{max}^2 \tag{29}$$

which we will call d_{lim}. Then, from equation 27 we can solve for r_{lim}, on a circular boundary,

$$r_{lim} = \sqrt{r_{max}^2 - d_{lim}^2} \tag{30}$$

and in turn, inverting equation 11, for $h_{c.max}$, the maximum available hour angle at the current setting,

$$h_{c.max} = \sin^{-1}\left[\frac{r_{lim}}{F_S \cos \delta_T} \right] \tag{31}$$

finally achieving an expression for the available tracking time (ATT), in hours, as follows:

$$ATT = \frac{24}{\pi} h_{c.max}. \tag{32}$$

ATT as a function of TDE is plotted in Figure 12.

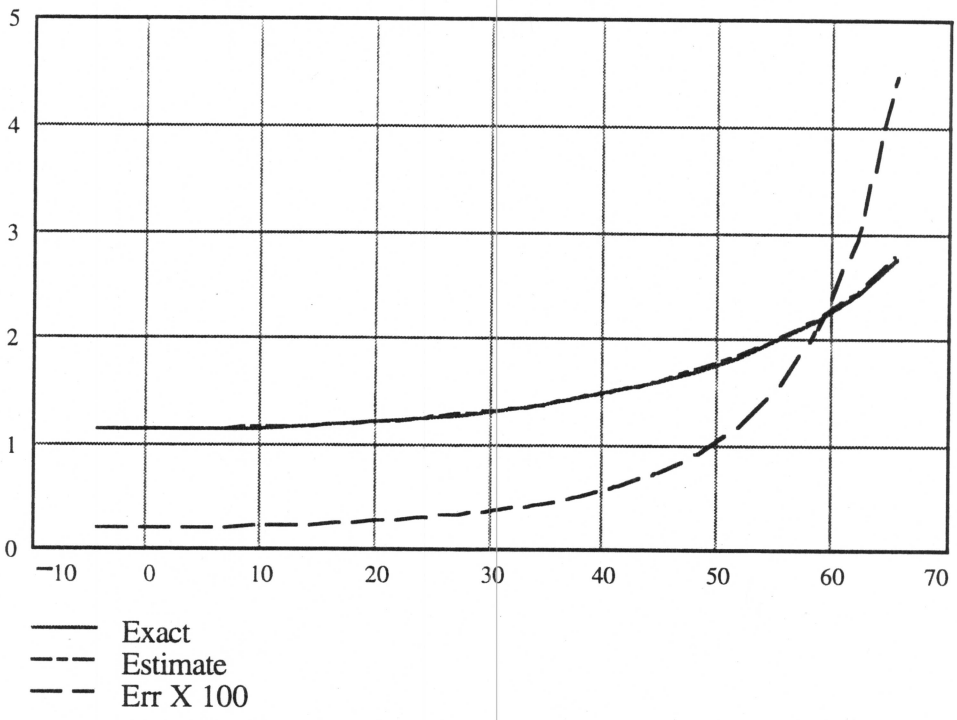

Figure 12. Available tracking time in hours for the SST's TDE range of -4.33° to 65.5°. The solid line indicates the exact calculation of time available for central trajectories only, the dash-dot line is an estimate assuming the trajectory has no projected curvature, and the dashed line is 100 times the error. The maximum error induced by ignoring trajectory curvature is about 4.5%.

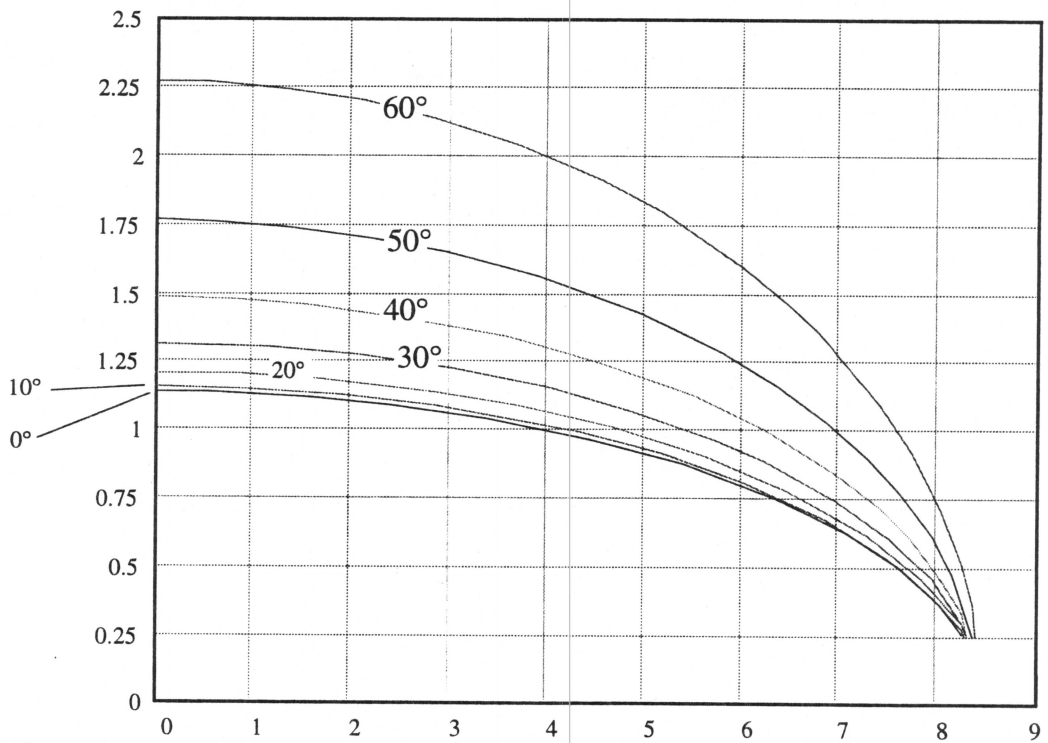

Figure 13. Attenuation of available exposure time, in hours, at TDEs ranging from 0° to 60°, for trajectory excursions off of the telecentric axis at the transit plane, in degrees.

Attenuation of the available tracking time, for the TDE range from 0 to 60 degrees, is plotted in Figure 13. This set of curves is calculated by defining r_{max} as a function of the trajectory's offset on the transit plane, which can vary from 0° to about 8.5° (represented by variable c in equation 29).

3.4 Vignetting

As the SST tracks, the entrance aperture defined by the corrector optics becomes de centered from the telecentric axis, and at about 1 meter lateral displacement at the primary mirror surface, the aperture begins to be vignetted. Figure 14 illustrates two principal directions for aperture excursion, and by symmetry at even and odd multiples of 30°.

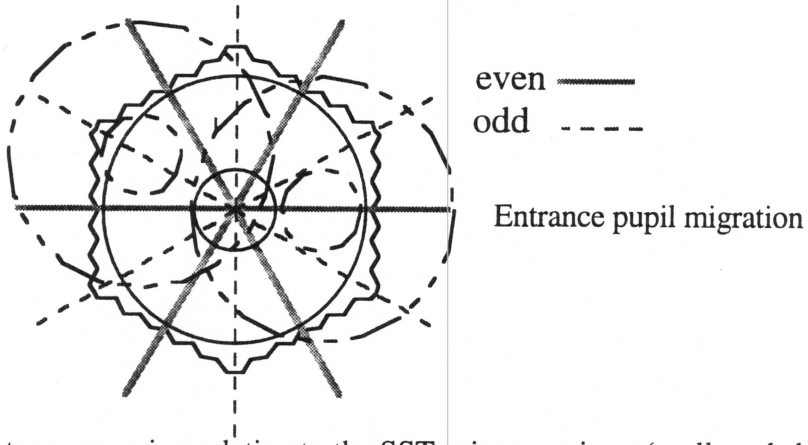

Figure 14. Aperture excursion relative to the SST primary mirror (scalloped shape). Vignetting is slightly different for the two principal directions (even and odd multiples of 30°).

An area attenuation function has been constructed for these principal directions, and is illustrated in Figure 15, in which percent area loss is plotted as a function of β, the distance of the line of sight from the telecentric axis. At a resolution of 0.25°, there is no useful difference in these two curves until angle β reaches about 7.5°, and certainly a linear interpolation between them would suffice for larger angles. It is important to note that an additional 17% area loss is incurred as the trajectory crosses the boundary of the 12° square and comes to an 8.5° circular limit.

For the data points generated for these curves, two separate cubic natural splines were fitted (the plots in Figure 15) and are integrated as interpolants in later continuous analyses to form a merit function for any given trajectory (for which β is available as a function of time, from equation 16), which gives the total area (and incident flux) encountered as a definite integral with respect to time.

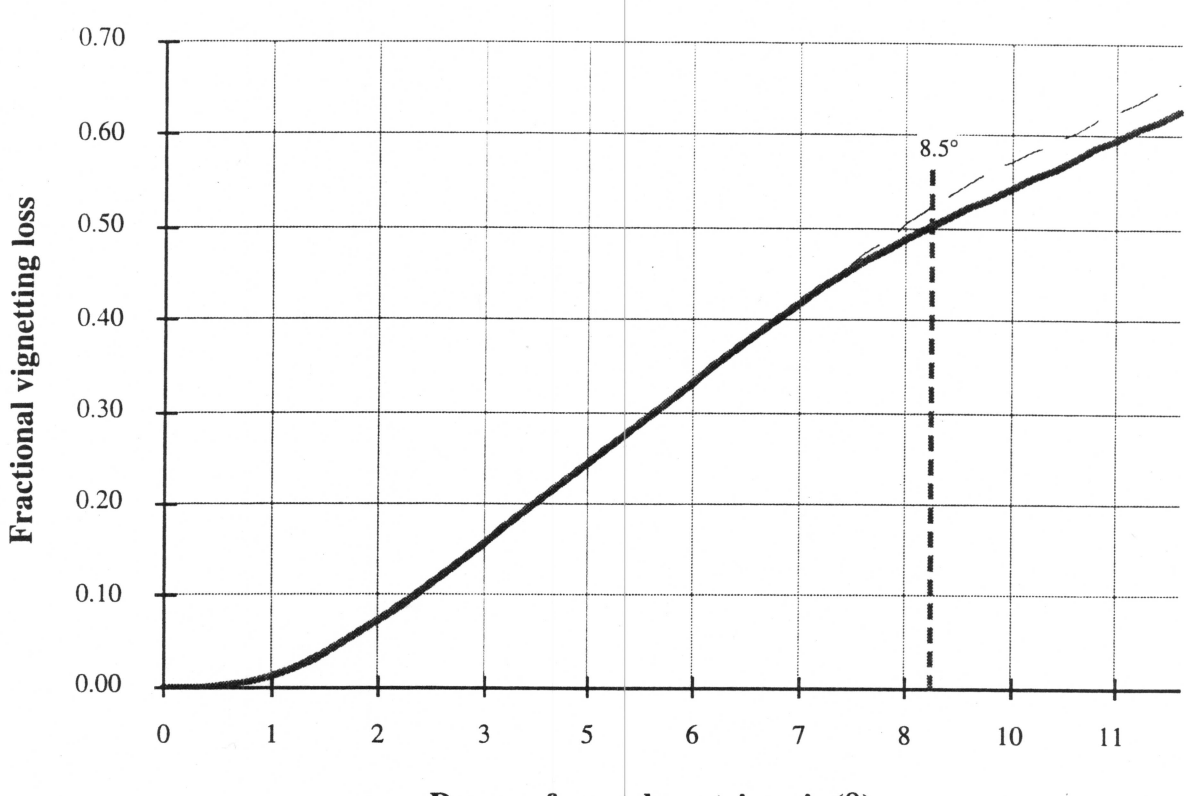

Figure 15. Even vignetting curve (solid) and odd (dashed).

If we define an aperture function

$$\mathcal{A}(t) = \mathcal{A}(\beta(t)) = \mathcal{S}(\text{area data}, (\beta(t))) \tag{33}$$

where $\mathcal{S}$ is the linearly interpolated result of the two cubic natural splines mentioned, then an area merit function, representing the total area encountered during a given trajectory, is given by

$$\mathcal{M}(t_o, x) = \int_{t_o}^{x} \mathcal{A}(\beta(t))\, dt \tag{34}$$

An example is plotted in Figure 16 for the trajectory shown in Figure 11, which is vignetted over its entire path. Plot 2 is less vignetted than plot 1, because of a better setting in azimuth, and therefore will require a shorter exposure time to obtain the same total incident flux for a given object.

This calculation suggests a mode of observing in which the observer requests the obtaining of spectra with a specified S/N ratio, leaving that task to a (computer-assisted) telescope operator.

The merit functions for these two are plotted in Figure 17. Definite integrals, comparing the exposure between the same limits (includes the peak areas) are as follows:

$$\int_1^2 \mathcal{A}1(t)dt = 0.891063 \qquad \int_1^2 \mathcal{A}2(t)\, dt = 0.946523 \tag{35}$$

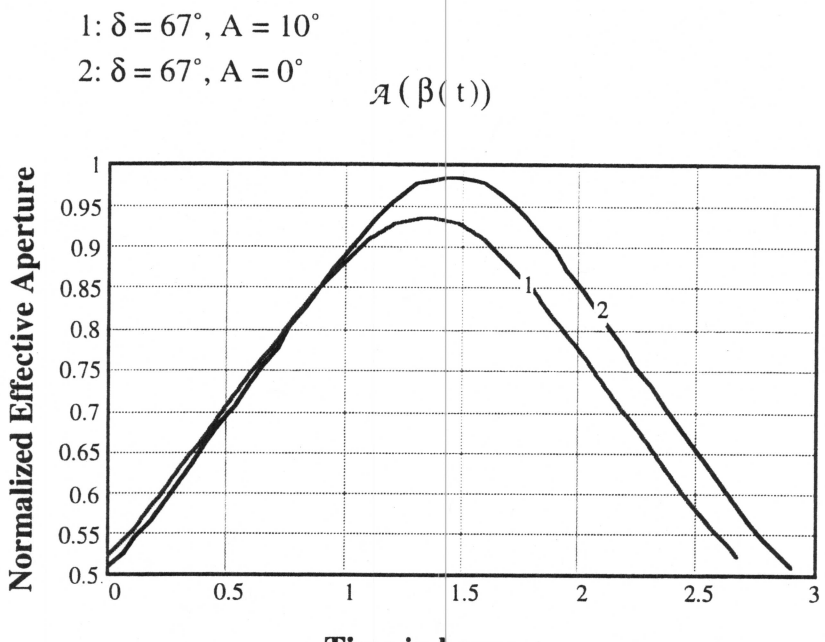

Figure 16. The aperture function $\mathcal{A}(\beta(t))$ plotted for the trajectory in Figure 11, with plot 1 at azimuth 10°, and plot 2 at azimuth 0°.

$$\mathcal{M}(t_0, x) = \int_{t_0}^{x} \mathcal{A}(\beta(t))dt$$

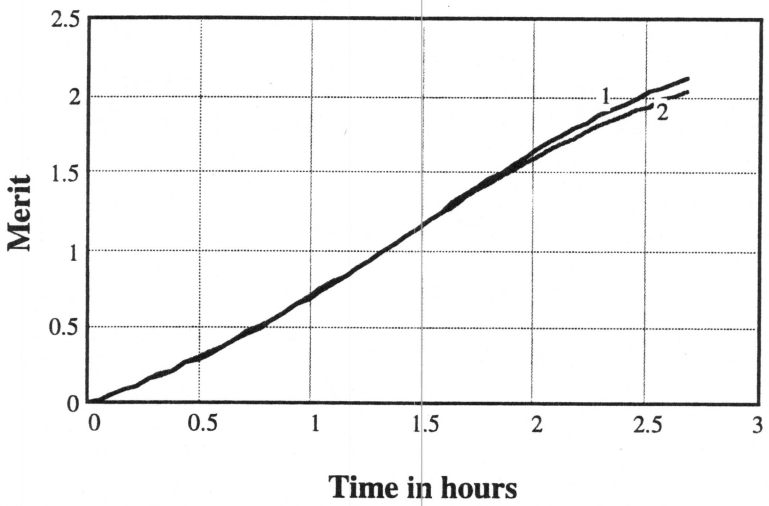

Figure 17. Merit functions for the same trajectory at two different azimuths.

3.5 Tracking rates

The time derivatives of equations 11 and 13 yield, noted as $\dot{r}$ and $\dot{d}$ respectively,

$$\dot{r} = F_S \left[\sin\delta \sin h_c \dot{\delta} - \cos\delta \cos h_c \dot{h} \right] \tag{34}$$

and

$$\dot{d} = F_S \, C2 \left[\sin\delta \cos h_c \dot{\delta} + \cos\delta \sin h_c \dot{h}_c \right] \tag{35}$$

where $\delta = \delta(t)$ and $h_c = h_c(t)$. Similarly, we can write the derivatives for x and y by differentiating equations 9 and 10, to obtain

$$\dot{x} = F_S \left[\left(\sin\delta \sin h_c \dot{\delta} - \cos\delta \cos h_c \dot{h_c} \right) \cos p_c - C2 \left(\sin\delta \cos h_c \dot{\delta} + \cos\delta \sin h_c \dot{h_c} \right) \right] \sin p_c \quad (36)$$

and

$$\dot{y} = F_S \left[\left(\sin\delta \sin h_c \dot{\delta} - \cos\delta \cos h_c \dot{h_c} \right) \sin p_c + C2 \left(\sin\delta \cos h_c \dot{\delta} + \cos\delta \sin h_c \dot{h_c} \right) \cos p_c \right] \quad (37)$$

These 4 rates are plotted in Figure 18.

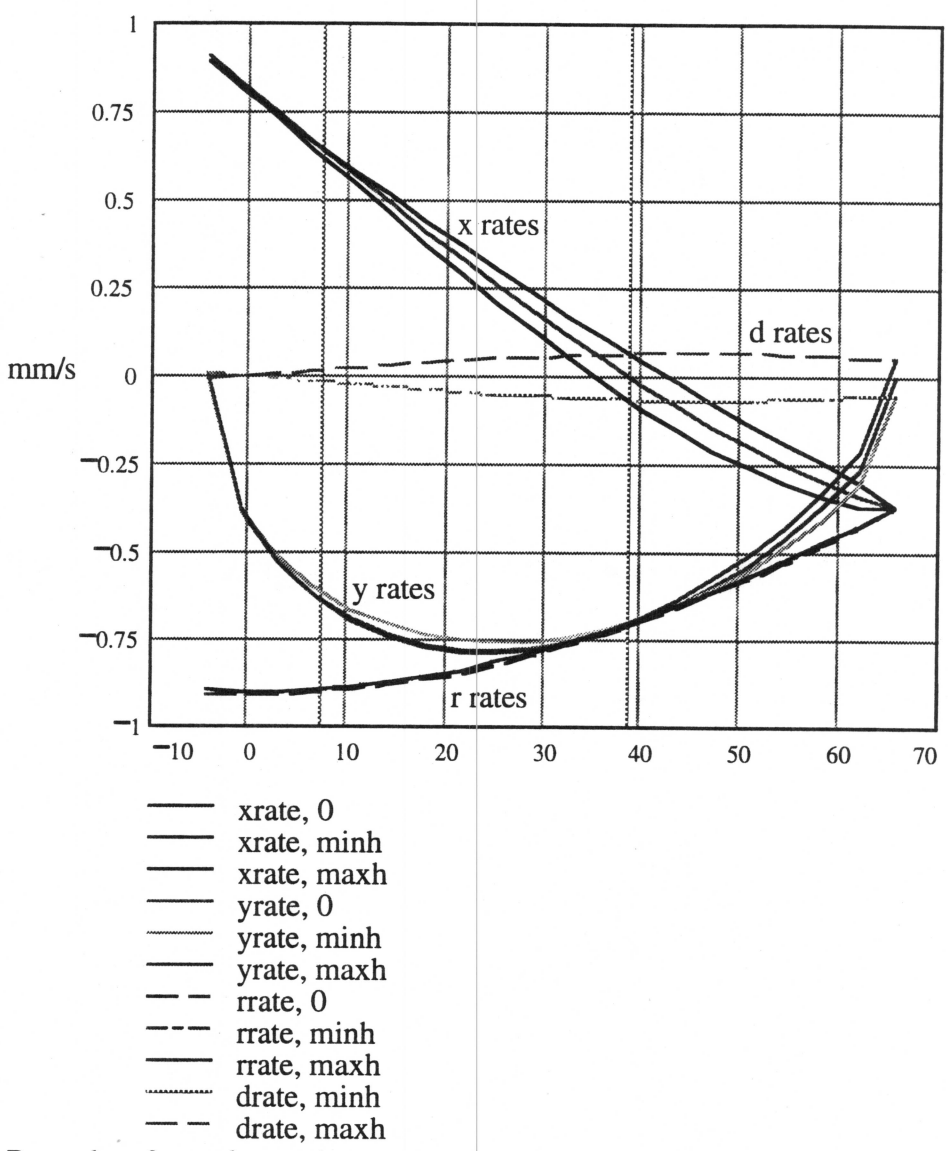

Figure 18. Rate plots for r, d, x, and y tracking coordinates, for central trajectories only. Tracking rates have a weak but non-negligible dependency on the variable h_c, or transit hour angle, indicated by the spread in each family of curves.

The rate for z, $\dot{z} = \dot{z}(t)$ is given by differentiating equation 18, using the previously derived functions for $\dot{x} = \dot{x}(t)$, $\dot{y} = \dot{y}(t)$, $x = x(t)$, and $y = y(t)$, as

$$\dot{z} = \frac{x\,\dot{x} + y\,\dot{y}}{\sqrt{F_S{}^2 - y^2 - x^2}} = \frac{x\,\dot{x} + y\,\dot{y}}{F_S - z} \tag{40}$$

Tilt rates for coordinates $\theta(t)$ and $\phi(t)$, about the X and Y axes, respectively, are given by the time derivatives of equations 19 and 20,

$$\dot{\theta} = \frac{F_S\left(\cos\beta\,\dot{y} + y\,\sin\beta\,\dot{\beta}\right)}{y^2 + (F_S\cos\beta)^2} \tag{41}$$

$$\dot{\phi} = \frac{F_S\left(\cos\beta\,\dot{x} + x\,\sin\beta\,\dot{\beta}\right)}{x^2 + (F_S\cos\beta)^2} \tag{42}$$

where by differentiating Equation 16 we have

$$\dot{\beta} = \frac{-\left[C2\cos\delta\,\dot{\delta} - C6\,(\cos h_c\sin\delta\,\dot{\delta} + \cos\delta\sin h_c\,\dot{h}_c)\right]}{\sqrt{1-(C2\sin\delta + C6\cos\delta\,\cos h_c)^2}} \tag{43}$$

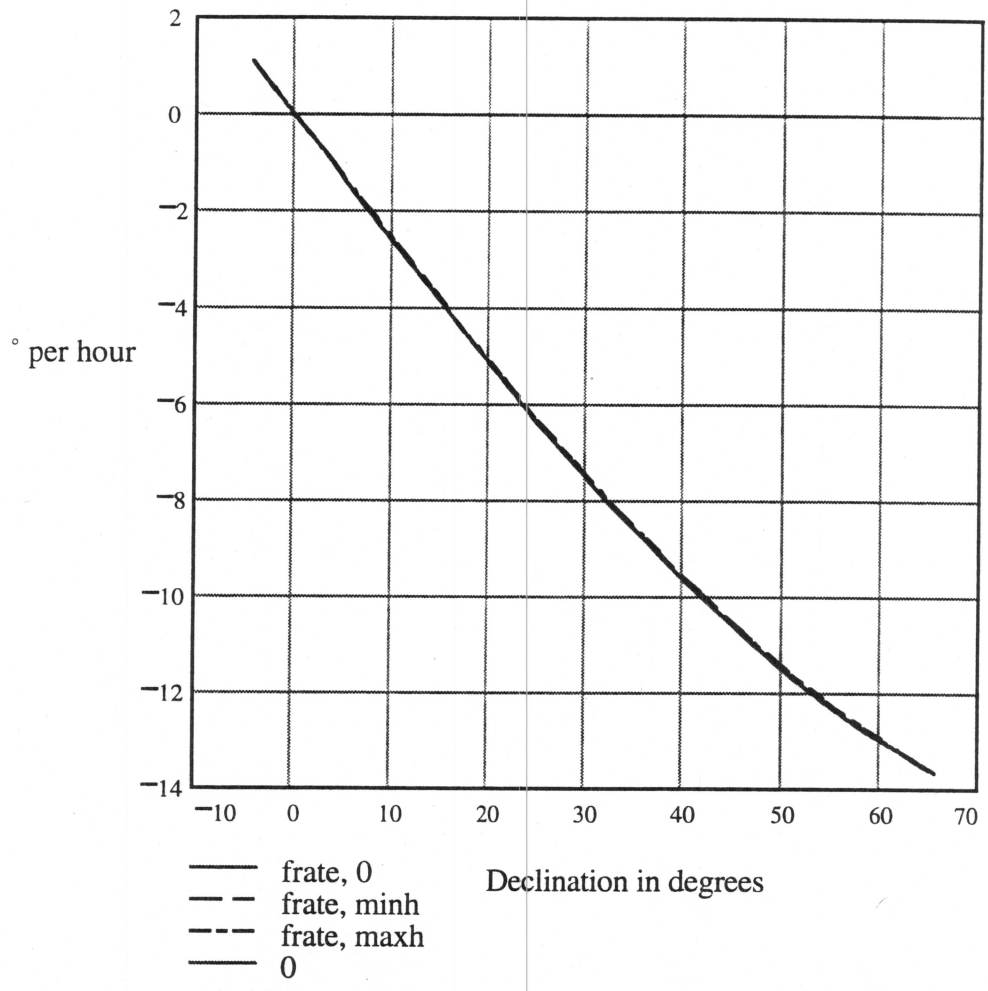

Figure 19. Field rotation rate $\dot{\rho}$ in degrees/hour as a function of declination and transit hour angle, showing an almost negligible dependence on h_c for each declination (and for sidereal rates).

Field rotation rate about the line of sight is given by the time derivative of equation 21

$$\dot{\rho} = \frac{-1}{\sqrt{1 - \sin^2 d \sin^2 h_c}} \left[\cos\delta \sin h_c \dot{\delta} + \sin\delta \cos h_c \dot{h_c} \right] \qquad (44)$$

and plotted in Figure 19. Note that the rate of field rotation is a function of declination and does not depend on *TDE* .

3.6 Rates for the tilting mechanism

For a Stewart Platform, or "hexapod" device, we assume 6 base, or fixed points, and 6 movable points. In either set, it is possible for the coordinates to converge, and we will treat each single point in that case as two points having the same coordinates. The fixed points are denoted by the labels F1, F2, . . . , F6, and the movable points by M1, M2, . . . , M6. We will assume that a variable length hexapod strut connects F1 to M1, F2 to M2, etc. We may express the position of the points M1 – M6 as a function of time by using the following transformation:

$$\{Mj'\}^T(t) = \{xMj', yMj' zMj', 1\}^T(t) = [\mathbf{TZ}](t)[\mathbf{T1}]^{-1}[\mathbf{R3}](t)[\mathbf{T1}]\ \{Mj\}^T\ , j = 1, 2 ,...., 6 \quad (45)$$

where [**TZ**](t) is a translation in the Z direction, defined by Eq. 17 or 18, [**T1**] controls the rotation point relative to the hexapod base, for example

$$[\mathbf{T1}] = \begin{bmatrix} 1 & 0 & 0 & -x_c \\ 0 & 1 & 0 & -y_c \\ 0 & 0 & 1 & -z_c \\ 0 & 0 & 0 & 1 \end{bmatrix} \tag{46}$$

and [**R3**](t) is a rotation matrix based on the values of $x(t)$, $y(t)$, and $z(t)$, such that, if

$$\zeta(t) = \sin^{-1}\left[\frac{\mathbf{y}(t)}{\mathbf{RV}_{YZ}(t)}\right], \left(\mathbf{RV}_{YZ}(t) = \sqrt{\mathbf{y}(t)^2 + (\mathbf{F}_S - \mathbf{z}(t))^2}\right), \psi(t) = \sin^{-1}\left[\frac{\mathbf{x}(t)}{\mathbf{F}_S}\right], \tag{47}$$

and

$$[\mathbf{RX}](t) = \begin{bmatrix} 1 & 0 & 0 & 0 \\ 0 & \cos\zeta(t) & -\sin\zeta(t) & 0 \\ 0 & \sin\zeta(t) & \cos\zeta(t) & 0 \\ 0 & 0 & 0 & 1 \end{bmatrix} \text{ and } [\mathbf{RY}](t) = \begin{bmatrix} \cos\psi(t) & 0 & -\sin\psi(t) & 0 \\ 0 & 1 & 0 & 0 \\ \sin\psi(t) & 0 & \cos\psi(t) & 0 \\ 0 & 0 & 0 & 1 \end{bmatrix} \tag{48}$$

then [**R3**](t) =[**RX**](t)[**RY**](t)as defined in report TR-940104[4].

Hexapod leg lengths, as a function of time, are then defined by the Euclidean distance

$$Hj(t) = \sqrt{(xFj - xMj'(t))^2 + (yFj - yMj'(t))^2 + (zFj - zMj'(t))^2}\ , j = 1, 2 ,..., 6 \tag{49}$$

where xFj denotes the x component of point Fj, and so on.

The function set {Hj, j = 1,2,...,6} is differentiated with respect to time to yield the rates for the hexapod legs, which are, in the compact notation defined previously,

$$\dot{Hj} = \frac{-1}{Hj}\left[(xFj - xMj')\,\dot{xMj'} + (yFj - yMj')\,\dot{yMj'} + (zFj - zMj')\,\dot{zMj'}\right], j = 1, 2 ,..., 6. \tag{50}$$

where the notation *$\dot{M}$j' abbreviates the time derivative of the * component of the jth hexapod leg of the product defined in Equation 45, or similar products, as defined in TR-940104. Note that only **TZ** and **R3** are time-dependent. For example, we can write formally the homogeneous derivative vectors

$$\{\dot{Mj'}\}^T(t) = \{\dot{xMj'}, \dot{yMj'}, \dot{zMj'}, 1\}^T(t) = [\dot{\mathbf{TZ}}](t)[\mathbf{T1}]^{-1}[\dot{\mathbf{R3}}](t)[\mathbf{T1}]\,\{Mj\}^T\ , j = 1,..., 6 \tag{51}$$

Various examples of tracking trajectories are illustrated at the end of this report. These include plots of coordinate rates for X, Y, Z, θ, ϕ, and ρ, as well as the six hexapod legs H1 – H6 based on a particular (rectangular) hexapod geometry. Similar rate functions may be likewise derived for the "wobble plate" mechanism described previously[5] in which a set of parallel screws provide the tilting motion.

---

[4] F. B. Ray, "Tracker mechanism kinematics, servo, and top-level software design for a semi-transit telescope with fixed spherical primary mirror", SST technical report TR-940104, January, 1994.
[5] ibid.

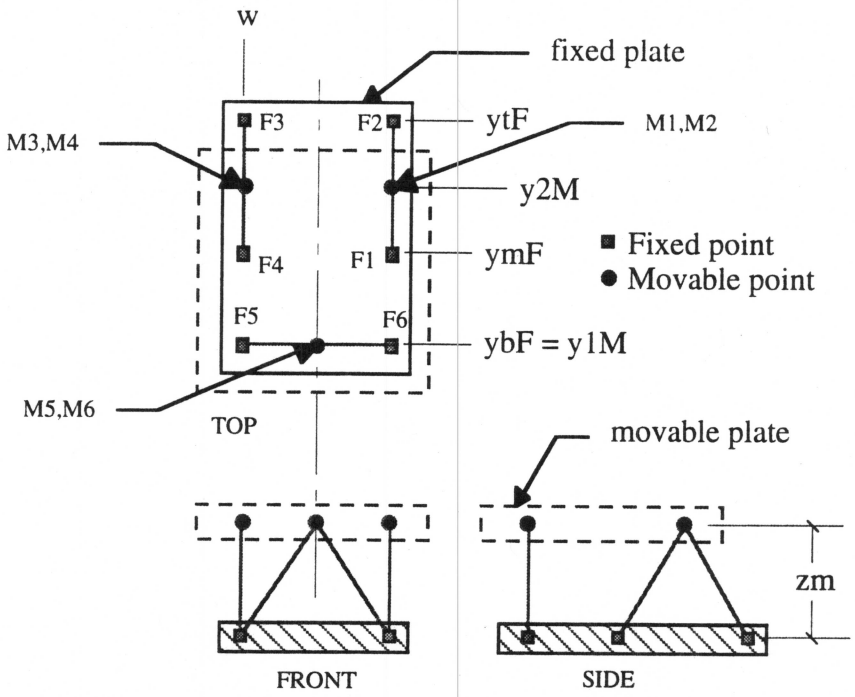

Figure 20. A rectangular hexapod geometry. The 6 points attached to the movable plate (M1–M6) have been condensed into 3 by means of special mechanical joints. Such an arrangement is more commensurate with the SST's XY rail configuration.

An example of (symmetric) rectangular hexapod geometry is shown in Figure 20. The Cartesian coordinates for all 12 points may be developed from such a layout. For the rates plotted in Figures 21–28, we have assumed w = 0.5m, zm = 1.0m, ybF = -0.5m, ymF = 0, ytF = 1.0m, and, assuming y2M is centered, y2M = (ymF + ytF)/2. The hexapod rates and accelerations generated are not overly sensitive to small changes in the geometry, and since the derivatives may be written in closed form, they are easily regenerated after a geometry change.

3.7 Acceleration

Given $\dot{x}$ and $\dot{y}$ as in Equations 36 and 37, we differentiate again to obtain the respective accelerations

$$\begin{aligned}\ddot{x} = F_S \big[&\big(\cos\delta \sin h_c \dot{\delta}^2 + 2\sin\delta \cos h_c \dot{h}_c \dot{\delta} \\ &+ \cos\delta \sin h_c \dot{h}_c^2 + \sin\delta \sin h_c \ddot{\delta} - \cos\delta \sin h_c \ddot{h}_c \big) \cos p_c \\ &- C2 \big(\cos\delta \cos h_c \dot{\delta}^2 - 2\sin\delta \sin h_c \dot{h}_c \dot{\delta} \\ &+ \cos\delta \cos h_c \dot{h}_c^2 + \sin\delta \cos h_c \ddot{\delta} + \cos\delta \sin h_c \ddot{h}_c \big) \sin p_c \big] \end{aligned} \tag{52}$$

and

$$\begin{aligned}\ddot{y} = F_S \big[&\big(\cos\delta \sin h_c \dot{\delta}^2 + 2\sin\delta \cos h_c \dot{h}_c \dot{\delta} \\ &+ \cos\delta \sin h_c \dot{h}_c^2 + \sin\delta \sin h_c \ddot{\delta} - \cos\delta \sin h_c \ddot{h}_c \big) \sin p_c \\ &+ C2 \big(\cos\delta \cos h_c \dot{\delta}^2 - 2\sin\delta \sin h_c \dot{h}_c \dot{\delta} \\ &+ \cos\delta \cos h_c \dot{h}_c^2 + \sin\delta \cos h_c \ddot{\delta} + \cos\delta \sin h_c \ddot{h}_c \big) \cos p_c \big] \end{aligned} \tag{53}$$

Similarly, differentiating the rate $\dot{z}$ again (Eq. 40) we arrive at the z acceleration

$$\ddot{z} = \frac{\dot{x}^2 + x\ddot{x} + \dot{y}^2 + y\ddot{y}}{\sqrt{F_S^2 - y^2 - x^2}} + \frac{(x\dot{x} + y\dot{y})^2}{(\sqrt{F_S^2 - y^2 - x^2})^3} \tag{54}$$

Acceleration of θ and ϕ is found from the derivatives of Equations 41 and 42; we therefore have

$$\ddot{\theta} = \frac{F_S \begin{pmatrix} -2y\cos\beta\ \dot{y}^2 - 2y F_S^2\cos\beta\ \dot{\beta}^2 \ldots \\ +2y F_S^2\cos^3\beta\ \dot{\beta}^2 + F_S^2\cos^3\beta\ddot{y} + y^2\cos\beta\ddot{y} \ldots \\ -y F_S^2\cos^2\beta\sin\beta\ddot{\beta} + y F_S^2\cos^3\beta\dot{\beta} - y^3\sin\beta\ddot{\beta} + y^3\cos\beta\dot{\beta} \end{pmatrix}}{F_S^4\cos^4\beta + 2F_S^2\cos^2\beta\, y^2 + y^4} \tag{55}$$

and

$$\ddot{\phi} = \frac{F_S \begin{pmatrix} -2x\cos\beta\ \dot{x}^2 - 2x F_S^2\cos\beta\ \dot{\beta}^2 \ldots \\ +2x F_S^2\cos^3\beta\ \dot{\beta}^2 + F_S^2\cos^3\beta\ddot{x} + x^2\cos\beta\ddot{x} \ldots \\ -x F_S^2\cos^2\beta\sin\beta\ddot{\beta} + x F_S^2\cos^3\beta\dot{\beta} - x^3\sin\beta\ddot{\beta} + x^3\cos\beta\dot{\beta} \end{pmatrix}}{F_S^4\cos^4\beta + 2F_S^2\cos^2\beta\, x^2 + x^4} \tag{56}$$

By differentiating Equation 50 a second time we can express the acceleration for the hexapod legs as

$$\ddot{H}j = \frac{-1}{Hj^3}\left[(xFj - xMj')\,\dot{xMj}' + (yFj - yMj')\,\dot{yMj}' + (zFj - zMj')\,\dot{zMj}'\right]^2 \ldots$$

$$- \frac{1}{Hj}\left[-\dot{xMj}'^2 + (xFj - xMj')\,\ddot{xMj}' - \dot{yMj}'^2 + (yFj - yMj')\,\ddot{yMj}' - \dot{zMj}'^2 + (zFj - zMj')\,\ddot{zMj}'\right],$$

$$\text{for } j = 1, 2, \ldots, 6, \tag{57}$$

where the derivatives $*\dot{M}j'$, * = x,y,z are defined in Equation 51 and the second (component-wise) derivatives are given by

$$\{\ddot{Mj}'\}^T(t) = \{x\ddot{M}j', y\ddot{M}j', z\ddot{M}j', 1\}^T(t) = [\ddot{\mathbf{TZ}}](t)[\mathbf{T1}]^{-1}[\ddot{\mathbf{R3}}](t)[\mathbf{T1}]\ \{Mj\}^T,\ j = 1,\ldots, 6 \tag{58}$$

3.8 Trajectory illustrations

Figure pairs (21,22) through (27,28) illustrate examples of position, rate, and acceleration for an "XYρ + hexapod" mechanism for several combinations of transit declination and azimuth.

TRAJECTORY

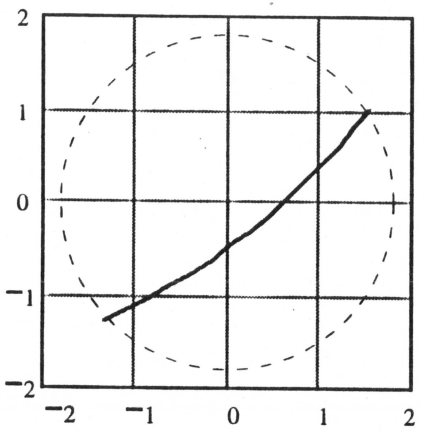

$\delta_T = 60 \cdot deg$

Az = 20 · deg T_D_E = 61.82 · deg

Par_Angle = 38.53 · deg

Time_available = 2.28 hours

RATES

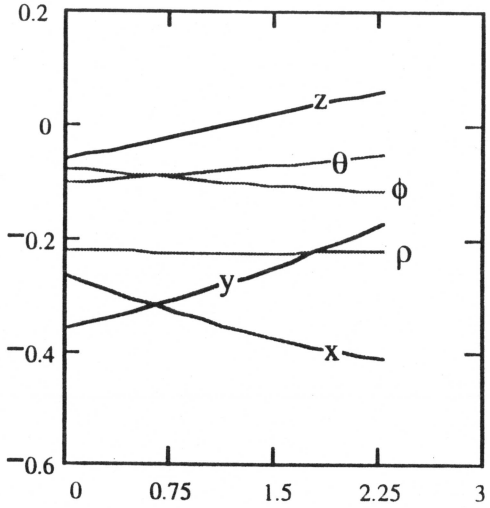

x.dot mm/s
y.dot mm/s
z.dot mm/s
theta.dot rad/hr
phi.dot rad/hr
FR.dot rad/hr

ACCELERATION X 1E06

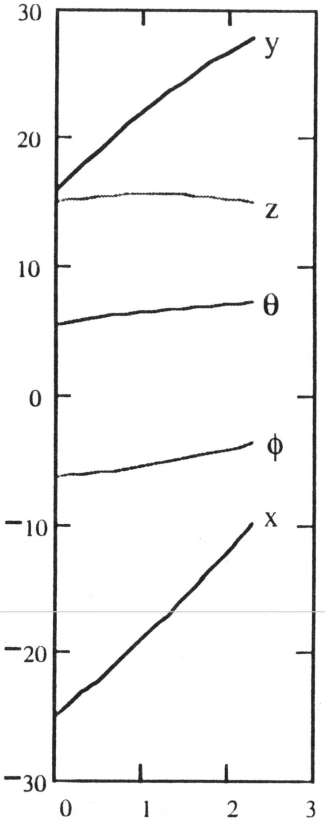

X Accel.
Y Accel.
Z Accel.
theta Accel.
phi Accel.

BETA IN DEGREES

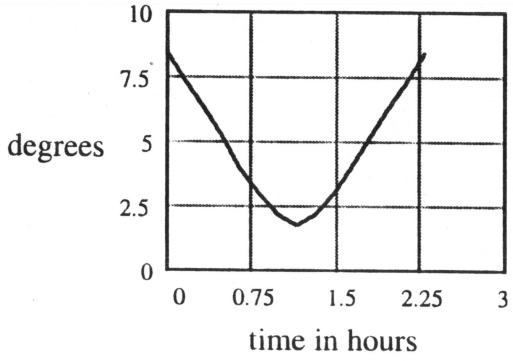

VIGNETTING LOSS

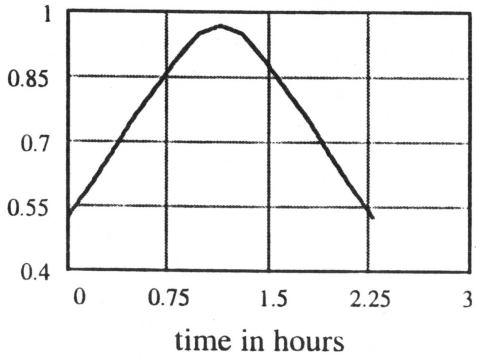

Figure 21

F. B. Ray, McDonald Obs., 4/4/94

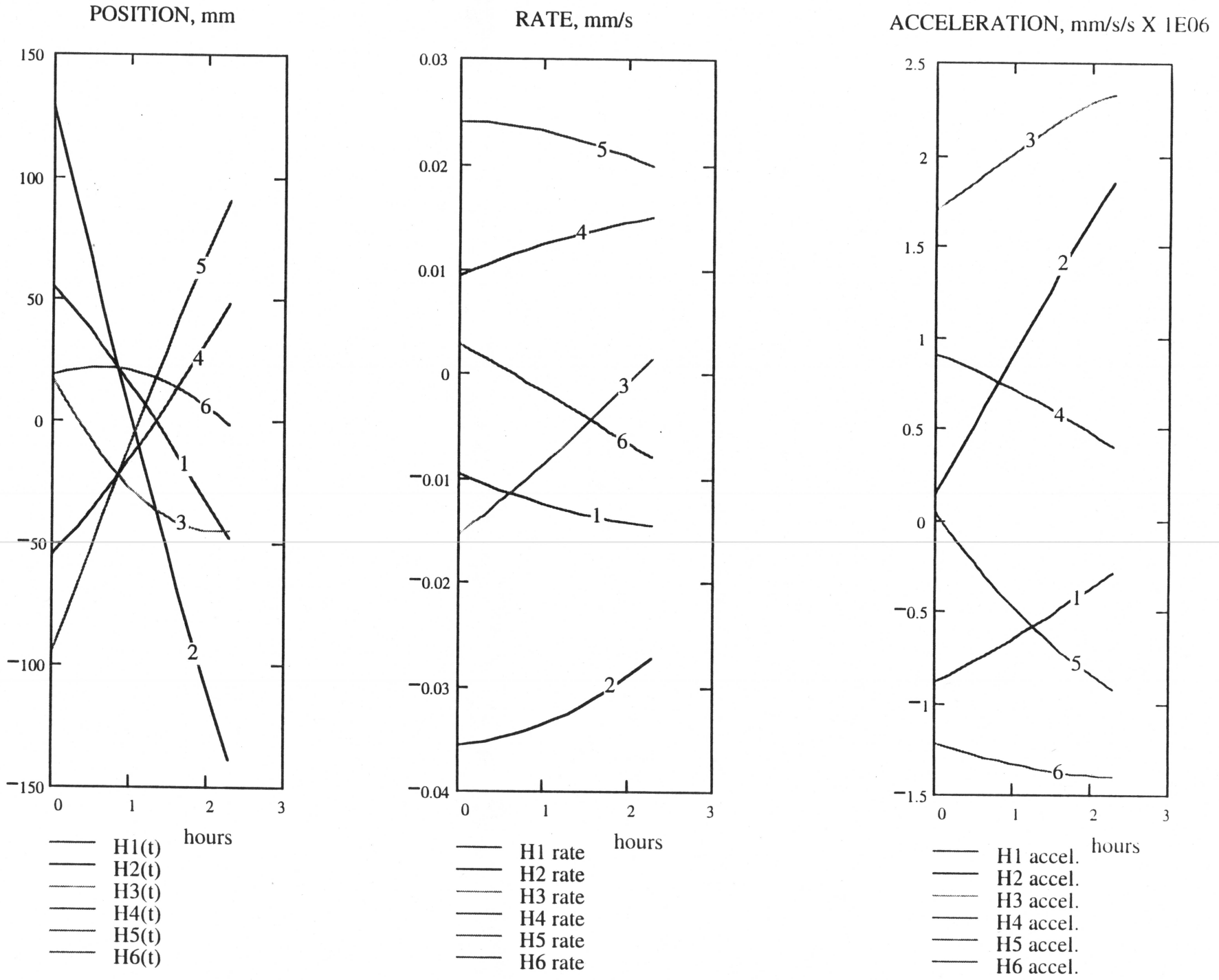

Figure 22

F. B. Ray, McDonald Obs., 4/1/94

TRAJECTORY

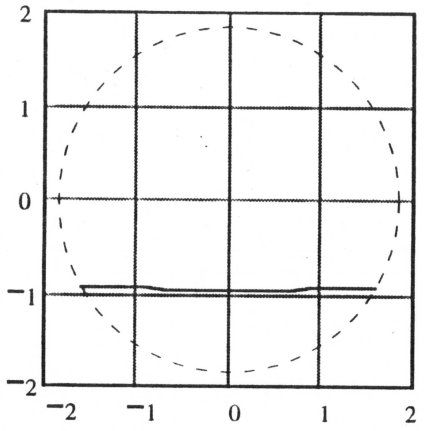

$\delta_T = 0 \cdot deg$

Az = 180 · deg T_D_E = −4.33 · deg

Par_Angle = 180 · deg

Time_available = 0.97 hours

RATES

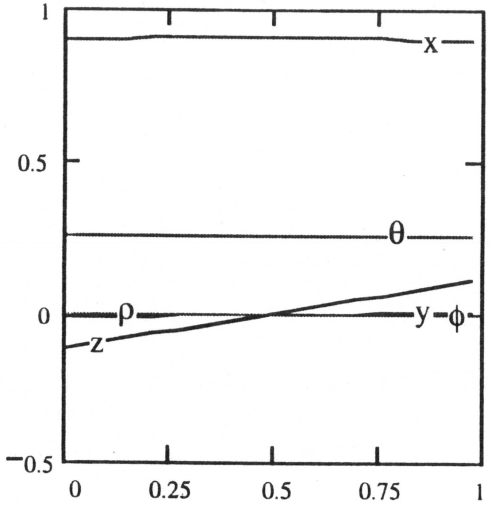

x.dot mm/s
y.dot mm/s
z.dot mm/s
theta.dot rad/hr
phi.dot rad/hr
FR.dot rad/hr

ACCELERATION X 1E06

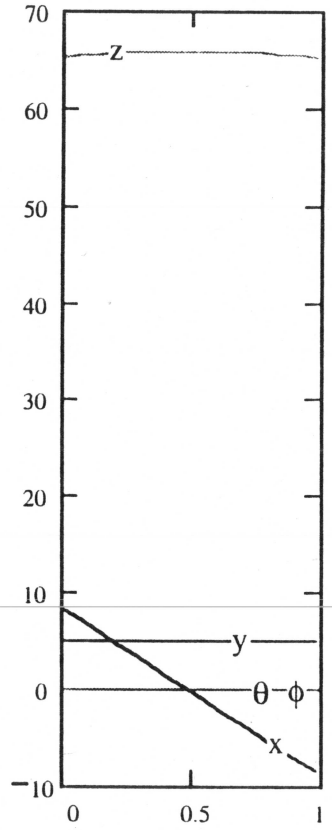

X Accel.
Y Accel.
Z Accel.
theta Accel.
phi Accel.

BETA IN DEGREES

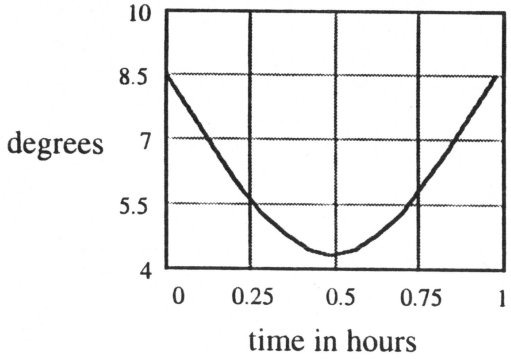

VIGNETTING LOSS

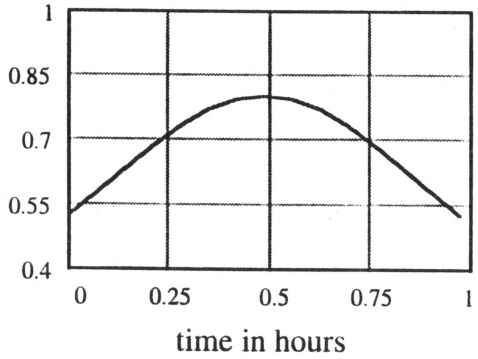

Figure 23

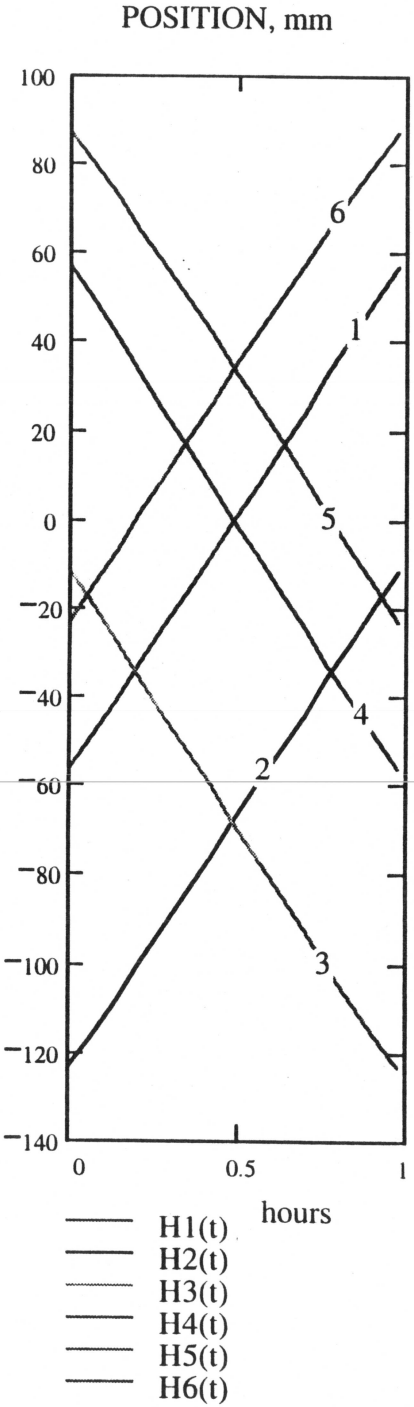

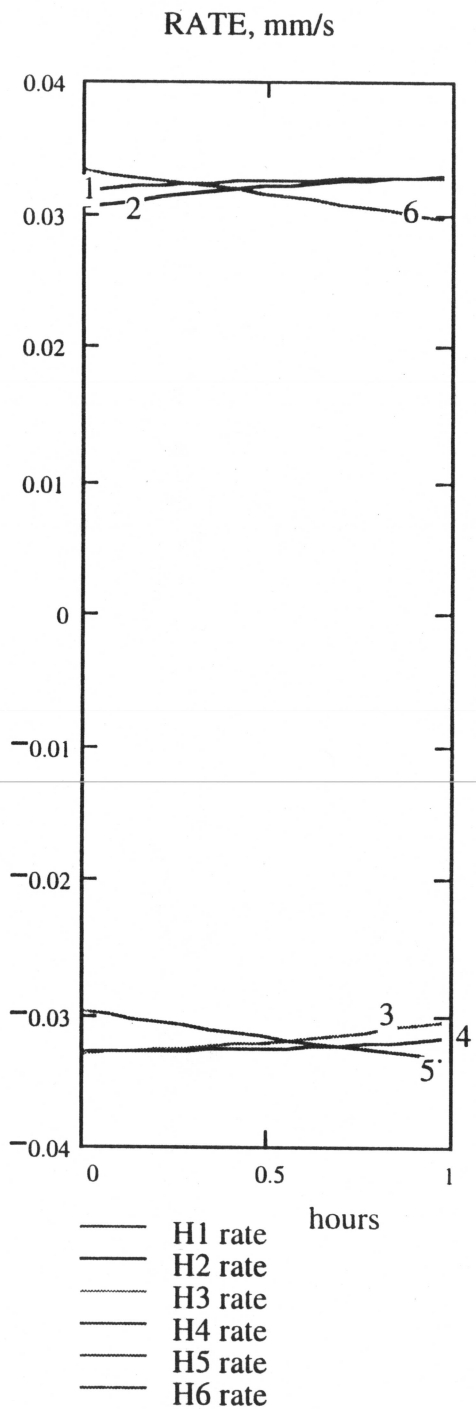

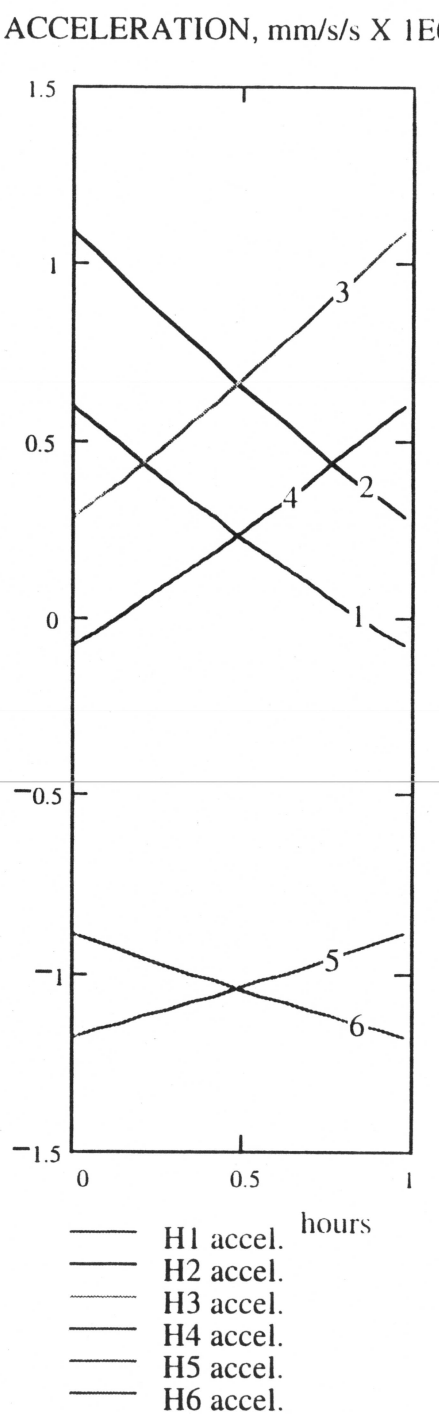

Figure 24

F. B. Ray, McDonald Obs., 4/1/94

TRAJECTORY

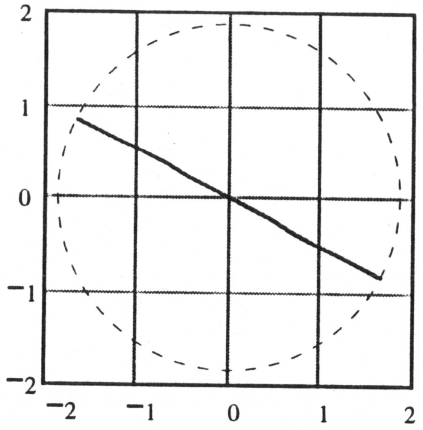

$\delta_T = 0 \cdot deg$

Az = 147.89 · deg T_D_E = 0 · deg

Par_Angle = 152.79 · deg

Time_available = 1.13 hours

RATES

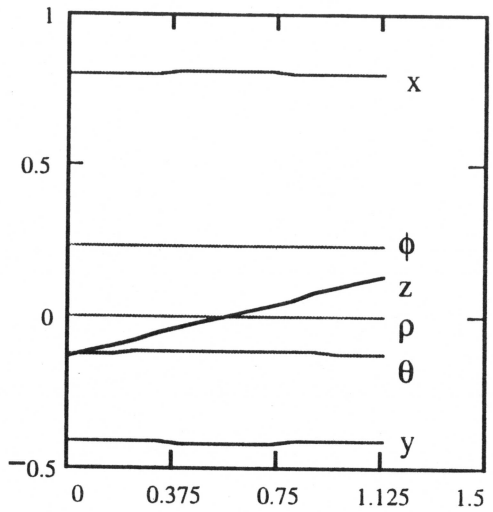

x.dot mm/s
y.dot mm/s
z.dot mm/s
theta.dot rad/hr
phi.dot rad/hr
FR.dot rad/hr

ACCELERATION X 1E06

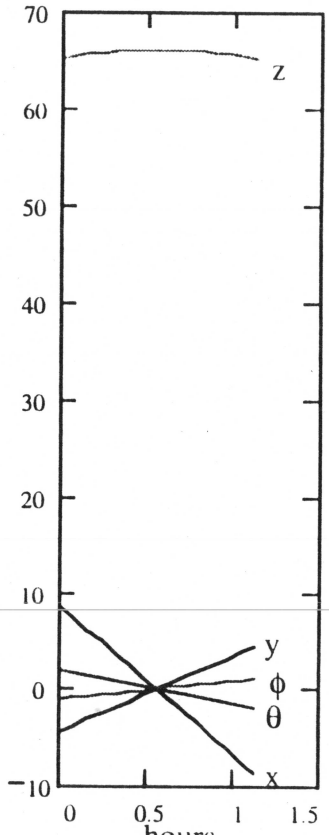

X Accel.
Y Accel.
Z Accel.
theta Accel.
phi Accel.

BETA IN DEGREES

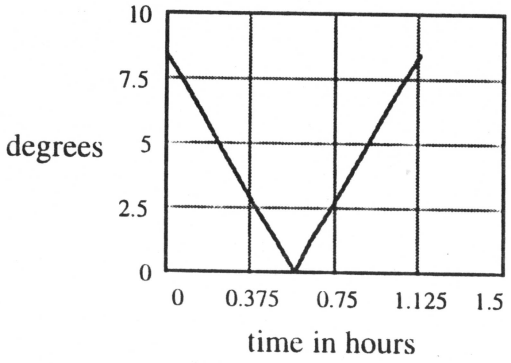

VIGNETTING LOSS

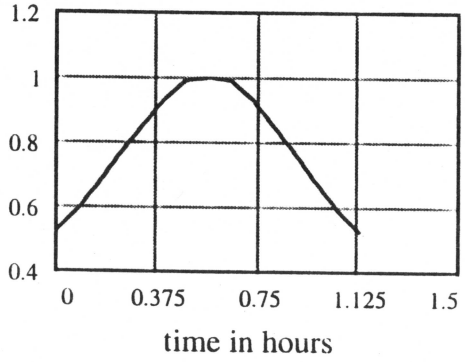

Figure 25

F. B. Ray, McDonald Obs., 4/1/94

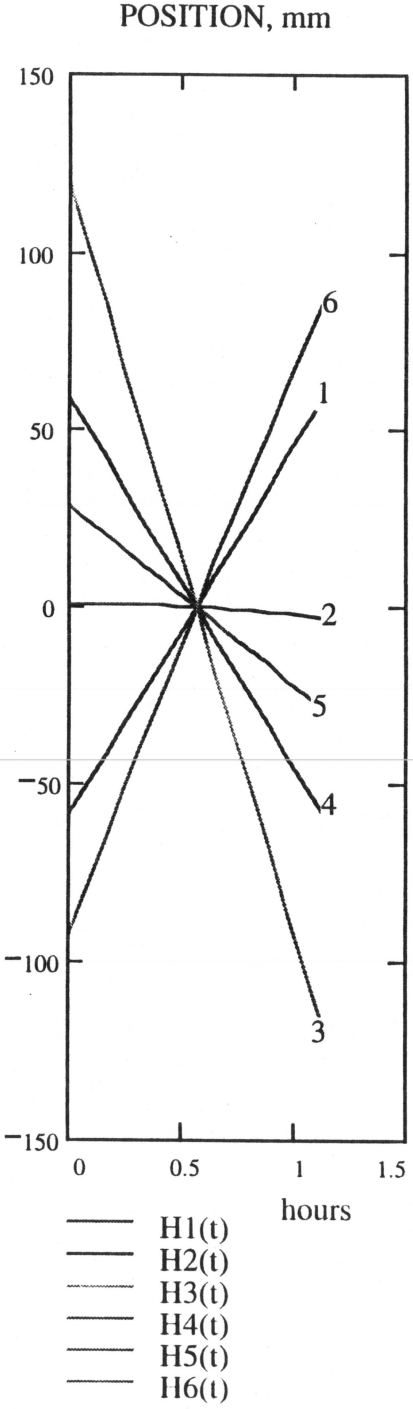

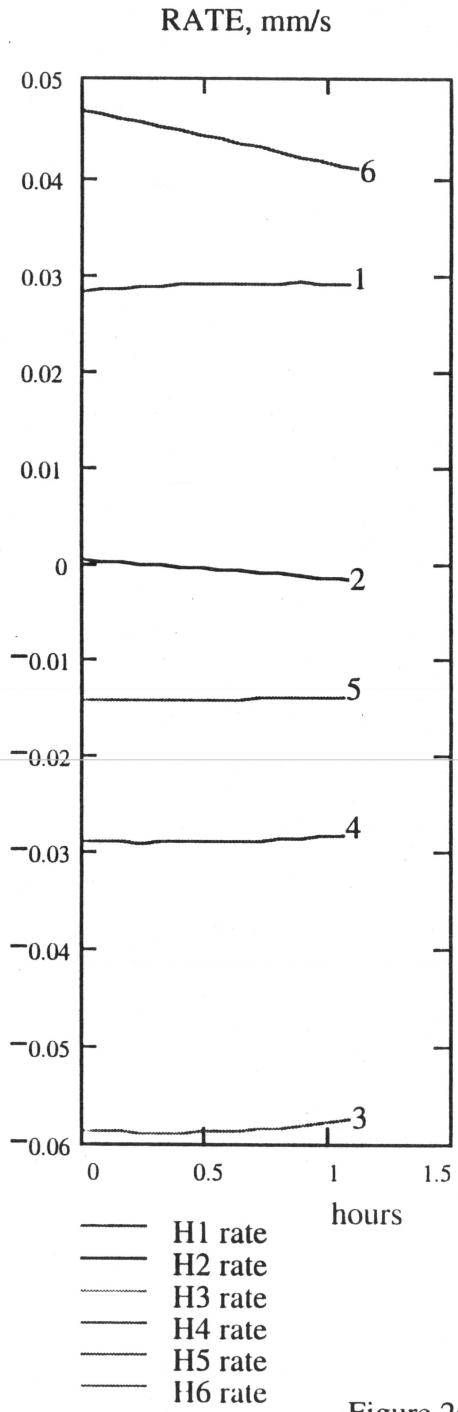

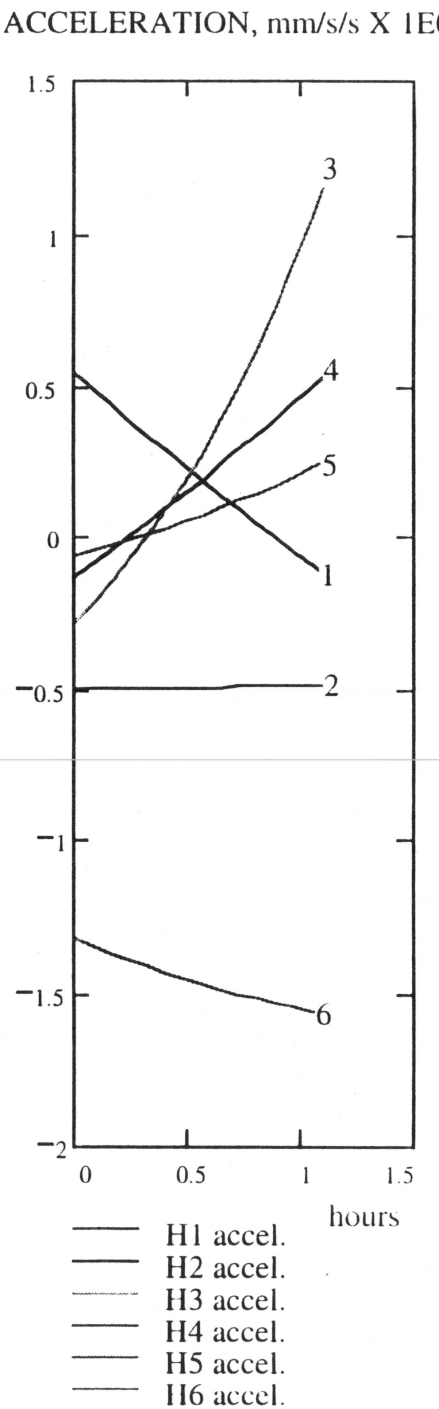

Figure 26

F. B. Ray, McDonald Obs., 4/1/94

TRAJECTORY

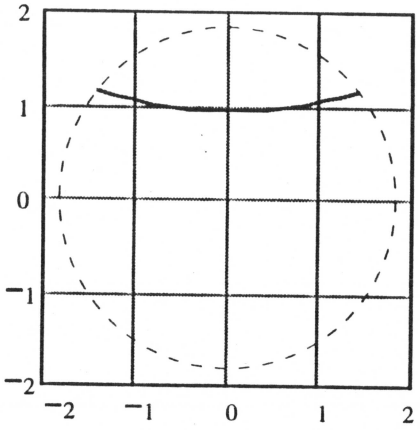

δ_T = 70 · deg

Az = 0 · deg T_D_E = 65.67 · deg

Par_Angle = 0 · deg

Time_available= 2.6 hours

RATES

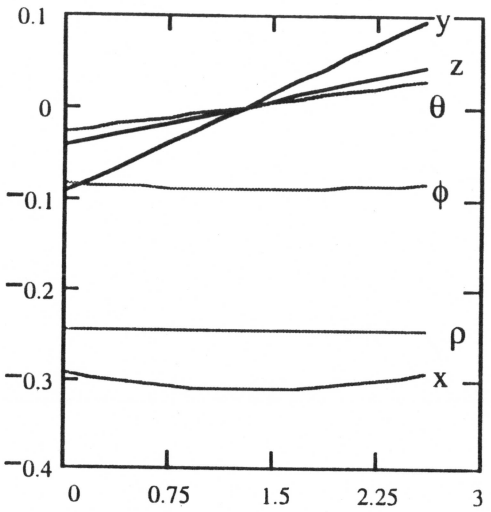

x.dot mm/s
y.dot mm/s
z.dot mm/s
theta.dot rad/hr
phi.dot rad/hr
FR.dot rad/hr

ACCELERATION X 1E06

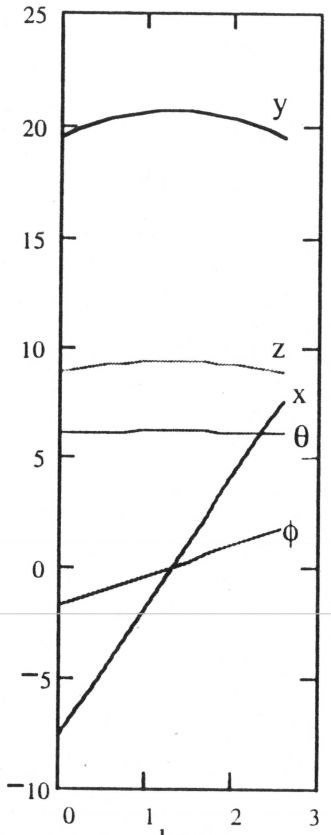

X Accel.
Y Accel.
Z Accel.
theta Accel.
phi Accel.

BETA IN DEGREES

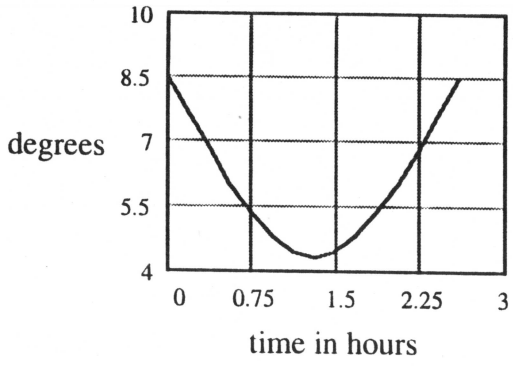

VIGNETTING LOSS

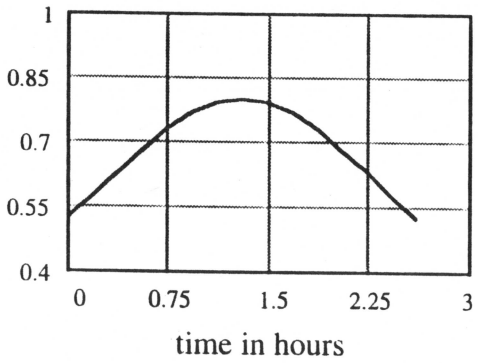

Figure 27

F. B. Ray, McDonald Obs., 4/1/94

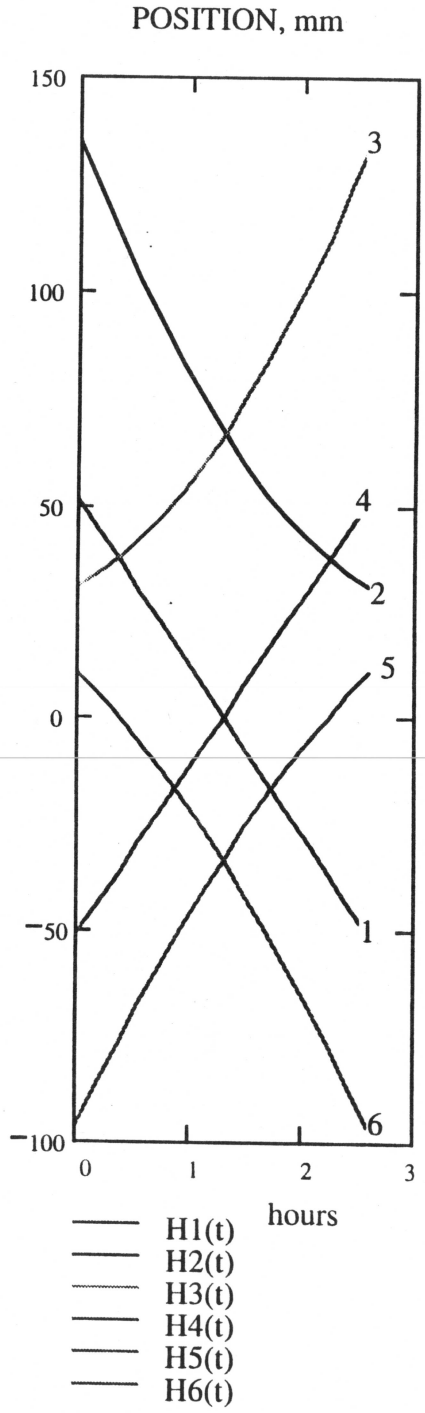

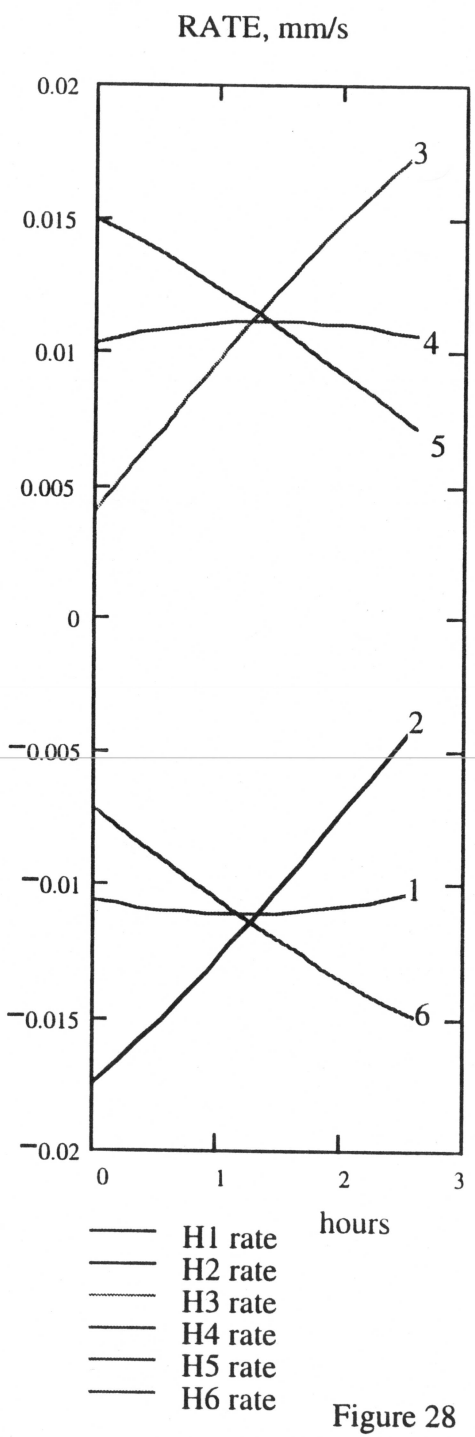

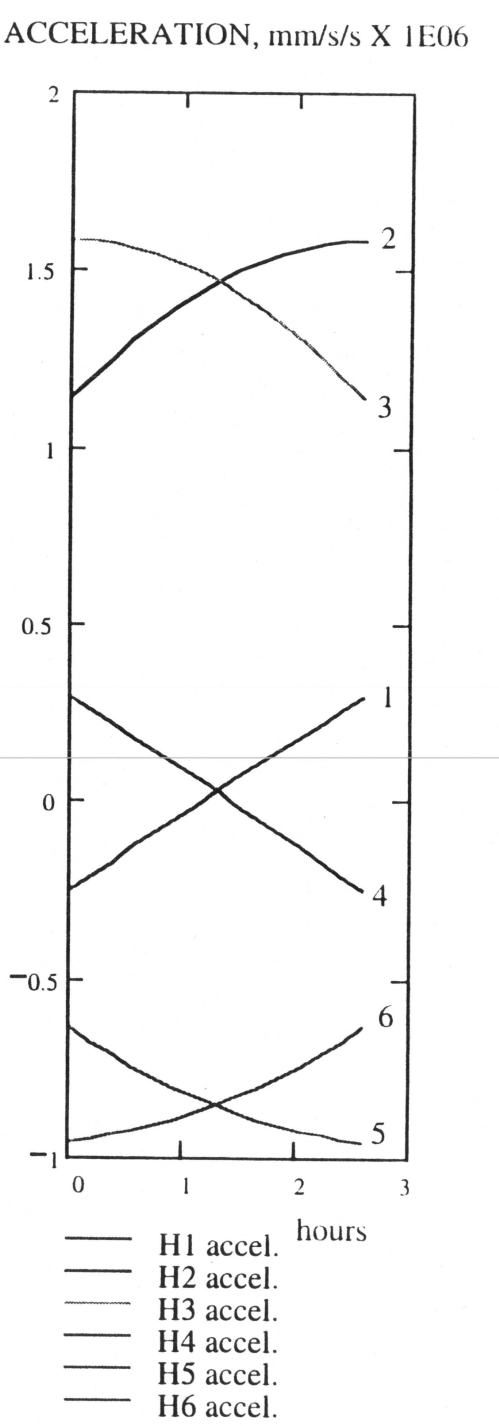

Figure 28

F. B. Ray, McDonald Obs., 4/1/94